EVALUATION OF TUMOR LOCALIZATION IN RESPIRATION MOTION-CORRECTED STEREOTACTIC BODY RADIOTHERAPY PATIENTS TREATED WITH TOMOTHERAPY

A DISSERTATION SUBMITTED TO THE GRADUATE DIVISION OF THE

UNIVERSITY OF HAWAI'I AT MĀNOA IN FULFILLMENT

OF THE REQUIREMENTS FOR THE DEGREE OF

DOCTOR OF PHILOSOPHY

IN

BIOMEDICAL SCIENCE

MAY 2017

BY

EMILY YUMEKO HIRATA

DISSERTATION COMMITTEE:

BEATRIZ RODRIGUEZ, CHAIRPERSON

THOMAS ERNST

JAMES DAVIS

SANDI KWEE

ALICE TSE

KEYWORDS: TOMOTHERAPY, STEREOTACTIC BODY RADIATION THERAPY, RESPIRATORY MOTION, LUNG CANCER

Acknowledgements

I am grateful to Dr. Rosanne Harrigan for her guidance and encouragement throughout my research career. Her unwavering support helped carry me through all the challenges and rough starts that I faced.

I would also like to expressly thank Dr. Ernst for his patience with me as I stumbled through my research. He never stopped encouraging me, and kindly pushed me to keep going even when I hit roadblocks and setbacks. I have learned so much from working with him and am indebted to his support.

I also want to thank all the students and the professors of the Clinical Research program who cheered me on throughout this journey. I especially appreciated the encouragement from Drs. Rodriguez, Tse, Davis, and Kwee for their guidance, compassion, and understanding.

I am indebted to the wonderful Medical Physics team at The Queen's Medical Center. They have always been a wonderful source of laughter, joy, and positivity, reminding me that it is important to pause from time to time and take stock of where I have been, where I am now, and where I am going. I work with the best team and could not imagine a better crew.

Last but not least, I'm thankful for the support and love of my family. My parents have always supported me and I am so incredibly lucky to be their daughter. I definitely could not have done this without Wesley, my husband, cheering me on and refusing to let me give up on this project, and my kids, Ryan and Jet, for their giddy laughter and bright smiles that remind me how much I have to be grateful for.

ABSTRACT

Lung cancer is the second most common cancer in both men and women, estimated to account for 158,080 deaths in 2016 according to the American Cancer Society(1). Approximately 85% of all lung cancers are non-small cell lung cancer (NSCLC). While surgical resection remains the standard therapy for operable stage I lung cancer patients(2), stereotactic body radiation therapy (SBRT) is a noninvasive alternative for the inoperable population(2–4).

SBRT is a technique that delivers high doses of radiation to tumors, generally in one to five treatments which are known as “fractions”. Since SBRT demands a high degree of confidence in tumor definition and localization, it requires the assessment and management of tumor motion (i.e. the respiratory excursion of the tumor)(3–7). Respiratory motion is of particular concern for TomoTherapy (Accuray, Inc, Sunnyvale, CA), which utilizes a continuously rotating gantry (maximum speed of 12 seconds per rotation) synchronized with a linearly moving couch to irradiate a target volume in a helical manner(8,9). The interplay between the motion of the radiation and the motion of the tumor can cause a discrepancy between the desired dose and the dose actually delivered. This is commonly referred to as the “interplay effect.” The goal of this work was to investigate the interplay effect using a cohort of patient respiratory waveforms and a motion phantom. Respiratory waveforms were characterized using principal component analysis of tumor displacement sampled via four-dimensional computed tomography (4DCT). These waveforms, programmed into the motion phantom were used to evaluate both the imaging and treatment accuracy of TomoTherapy. Ion chamber and film measurements were collected for the static condition, motion at the native breath frequency of the patient, and a modified motion averaging 5 breaths per minute (bpm).

TomoTherapy megavoltage CT (MVCT) scans did not show marked interplay effect. Scanning in fine mode resulted in smaller positional errors, though larger imaging artifacts were visible. Lower breath frequencies were significantly associated with larger variance in dose, and larger amplitude of tumor displacement correlated with larger penumbral blurring. Banding of hot and cold were observed on film for several cases, although ion chamber measurements were mostly within the recommended 2% criteria.

Strategies for minimizing the interplay effect involve maintaining an elevated breath frequency, improving regularity of the respiratory waveform, and avoiding the use of TomoTherapy plans with a fast

gantry period of 12 seconds per rotation. The results of this dissertation provide a clinically based evaluation of the interplay effect on TomoTherapy for SBRT treatments.

Table of Contents

List of Tables

List of Figures

List of Abbreviations

3DCT	3-Dimensional Computed Tomography
4DCT	4-Dimensional Computed Tomography
AAPM	American Association of Physicists in Medicine
AP	Anterior-Posterior
ASTRO	American Society for Therapeutic Radiation Oncology
BED	Biological Effective Dose
BPM	Breaths Per Minute
CT	Computed Tomography
CTV	Clinical Tumor Volume
D95	Dose to 95% volume of the planning target volume
DICOM	Digital Imaging and Communications in Medicine
Dmax	Maximum Dose
Dmin	Minimum Dose
IMRT	Intensity Modulated Radiation Therapy
ITV	Internal Target Volume
LINAC	Linear Accelerator
MVCT	Mega-Voltage Computed Tomography
MRN	Medical Record Number
NSCLC	Non-Small Cell Lung Cancer
PTV	Planning Target Volume
QA	Quality Assurance
QMC	The Queen's Medical Center
RL	Right-Left
SBRT	Stereotactic Body Radiation Therapy
SCLC	Small Cell Lung Cancer
SI	Superior-Inferior
SD	Standard Deviation

Chapter 1 Introduction and Specific Aims

1.1 Introduction

According to the American Cancer Society lung cancer is the leading cause of death for both men and women, responsible for approximately 158,080 deaths in the United States in 2016(15). Treatment for lung cancer depends on many factors, including the type of cancer, how far it has spread, and the individual's performance status. Common treatments include palliative care, surgery, chemotherapy, immunotherapy, and radiation therapy, often used in combination.

Among these options, a radiation therapy technique that is growing in use is stereotactic body radiotherapy (SBRT). SBRT delivers high doses of radiation to the tumor in 1 to 5 fractions, and is a potential option for people ineligible for surgery. The large doses of radiation require a higher degree of accuracy for each treatment. A geometric miss resulting in a reduction in tumor dose for any one fraction may significantly reduce the overall treatment effectiveness or significantly increase the risk of complications if critical organs received higher doses than anticipated. Respiratory motion presents an additional challenge for lung tumors. As patients breathe, lung tumors move – some up to 1-2 cm in the lower lobe. Additionally, patients exhibit a variety of respiratory patterns, where some breathe in a regular sinusoidal fashion, while others inhale quickly followed by a long slow exhale. Other respiratory patterns may be irregular, without a strong inhale or exhale. An effective SBRT program must account for tumors that move under a variety of respiratory patterns, and still maintain accurate dose delivery to achieve expected treatment outcomes.

One technologically advanced system used in radiation therapy, including SBRT, is TomoTherapy (Accuray, Inc, Madison, WI). TomoTherapy is a radiation delivery system with integrated imaging that delivers tiny beamlets of radiation using a continuously rotating gantry-mounted 6 MV linear accelerator. Radiation is delivered in a slice-by-slice fashion as the gantry rotates helically around the patient. While TomoTherapy can delivery highly conformal radiation doses, there are concerns regarding the potential synchrony of the helical delivery approach with a moving target resulting in underdosing the target volume or overdosing critical organs; this is referred to as the "interplay effect."

The interplay effect occurs when the radiation delivery is out of phase with the moving lung tumor. Because radiation is delivered serially along the superior-inferior axis of the patient, it is theoretically possible for the lung tumor to move in such a way that it is out of the beam for a significant percentage of time.

The interplay effect can adversely impact SBRT treatment effectiveness in two ways: 1) reducing the imaging accuracy for patient positioning prior to treatment, and 2) reducing the dose actually delivered to the tumor. While several studies have evaluated the interplay effect with SBRT, no study has incorporated actual patient respiratory traces. The goal of this study is to characterize the interplay effect using a motion phantom, programmed with patient respiratory patterns and tumor displacements, and a spectrum of imaging and treatment parameters.

1.2 Specific Aims and Hypotheses

The interplay effect for both Imaging and treatment on the TomoTherapy system for SBRT has yet to be characterized with a population of patient respiratory waveforms that represent a snapshot of each patient's breathing motion. This study evaluates the interplay effect in patients treated with SBRT with TomoTherapy with the following aims:

Aim 1: Characterize the respiratory motion in a cohort of patients with lung cancer

Aim 2: Determine the effect of a patient's breath frequency and tumor displacement on the accuracy of the TomoTherapy image acquisition (MVCT) system.
Hypothesis: Higher breath frequencies and larger amplitudes will lead to errors in the MVCT localization of the tumor

Aim 3: Determine the effect of a patient's breath frequency and tumor displacement on the accuracy of the TomoTherapy treatment delivery.
Hypothesis: Higher breath frequencies and larger amplitudes will reduce the tumor dose

Aim 4: Examine methods to match treatment planning parameters (ie. Pitch) with breath frequencies to minimize the interplay effect.
Hypothesis: Use of a larger pitch will improve the accuracy of the treatment

1.3 Statistical Methods

Statistical analysis for this dissertation was performed using R (R Core Team 2013). Paired t-tests were conducted to determine statistically significant differences in positional shifts, volume, and dose differences between the stationary and motion conditions. Independent-samples t-tests were used to evaluate measurements stratified by fast and slow breath frequencies, and high and low tumor amplitudes for both the native-breath frequency and 5-bpm cohorts. For standard deviation comparison, both a paired t-test and Wilcoxon rank sum test were performed. Scatter plots and box plots were generated to illustrate the results in each section, and p-values were noted for each result.

1.4 Organization of the Dissertation

In Chapter 2, a literature review on the topic of SBRT and the challenge of respiratory motion is presented. In Chapter 3, a brief review of the TomoTherapy system is presented as well as a literature review of the interplay effect.

Chapters 4, 5, 6, and 7 summarize the main experiments performed as part of this dissertation. In Chapter 4, characteristics of respiratory waveforms used in this dissertation are presented. The

techniques used to program the motion phantom are also discussed. Chapter 5 presents the results of the imaging component of this study, evaluating the impact of different respiratory waveforms and breath frequencies on the images acquired by the TomoTherapy system. Chapter 6 presents the results of the dose delivery study to determine how the respiratory waveforms and breath frequencies affect the dose delivered to a moving target using an ion chamber and film. Chapter 7 evaluates the impact of the interplay effect when the pitch of a plan is varied.

Finally, Chapter 8 summarizes and synthesizes the findings in this dissertation, identifies ways to optimize the treatment delivery with a patient's respiratory characteristics, and discusses the limitations of the work presented. Potential areas of future research are also identified in this chapter.

Chapter 2 Background and Literature Review

2.1 Overview

Lung cancer is the second most common cancer in both men and women, estimated to account for 158,080 deaths in 2016 according to the American Cancer Society (1). In addition, it is estimated that 224,390 new cases of lung cancer were expected to be diagnosed during 2016; worldwide, lung cancer accounted for 1.8 million new cases and 1.6 million deaths in 2012 (16).

There are two main types of lung cancer: non-small cell lung cancer (NSCLC) and small cell lung cancer (SCLC). Approximately 85% of all lung cancers are non-small cell lung cancer (NSCLC). Surgical resection of early-stage (stage I, II) NSCLC is the standard against which other therapies are compared (2). According to the American Cancer Society, the average age at the time of lung cancer diagnosis is around 70 years old, and two out of 3 adults diagnosed with lung cancer are over the age of 65. Less than 2% of patients are younger than 45 years old at the time of diagnosis. For this reason, many patients will be ineligible for surgery, or may have other comorbidities such as poor pulmonary or cardiovascular function. Historically, the options available to these patients were watchful waiting or conventional radiotherapy. The outcomes of these approaches are generally poor (17,18).

Another challenge is the treatment of thoracic recurrence, especially if prior radiation was given. Jeremic *et al.* reported thoracic recurrences or new metachronous primary lung tumor occurred roughly in the range of 4-10% (19). With the latest advances in imaging technology and the ability to deliver large doses to small volumes of tumor, SBRT is used to not only treat primary lung cancer, but also recurrent disease and has significantly improved the local control rates in lung cancer (20,21).

2.2 Stereotactic Body Radiotherapy (SBRT)

Stereotactic body radiotherapy, also known as stereotactic ablative radiotherapy, delivers high doses of radiation, by aiming several beams of radiation at the tumor from different angles. SBRT treatment regimens can be a single fraction in one day, or up to five fractions delivered over the course of 1-2 weeks, depending on the patient's physical condition, the type of tumor, and the location of the tumor. A commonly used method to compare the different fractionation schemes is the biologically effective dose (BED). The BED is based on the linear quadratic (LQ) equation, a widely-accepted model of cell kill by radiation:

(1) $$LQ\ Equation: \quad S(D) = e^{-\alpha D - \beta D^2}$$

S(D) is the fraction of cells that survive a dose D, α and β are constants that describe the linear and quadratic components of cell killing respectively. The BED is derived from this LQ equation and represents the biological dose delivered by a combination of dose per fraction and total dose to a

particular tissue, with each tissue characterized by a parameter called the α/β ratio. The equation for BED is:

(2) $$BED = nd\left[1 + \frac{d}{\alpha/\beta}\right]$$

where n is the number of fractions, d is the dose per fraction, and the α/β ratio is the dose where cell killing from the linear and quadratic components are equal. A commonly used α/β ratio is 10 Gy for tumors, and 3 Gy for normal tissues. Some examples of commonly used SBRT doses are described in Table 1. Reaching a high BED has been shown to improve overall survival, with local tumor control rates exceeding 90% at 3 years (18). The effectiveness of SBRT is generally attributed to achieving a BED > 100 Gy (22–24), while maintaining a sharp dose fall off outside the target, thereby salvaging nearby critical organs. However, Koshy *et al*. evaluated the comparative effectiveness of different SBRT dose fractionations for early-stage NSCLC from the National Cancer Database from 2003-2006, and concluded that patients who received a BED >150 Gy had a significantly improved survival (7). The debate regarding the optimal SBRT dose fractionation between tumor eradication and toxicity remains ongoing.

Table 1. Common SBRT dose fractionation.
Examples of common SBRT dose fractionation schemes with associated biological effective dose (BED).

Common SBRT dose fractionation			
Total Dose (Gy)	No. Fractions	Dose per Fraction (Gy)	BED (Gy)
60	5	12	132
48	4	12	106
54	3	18	151
60	3	20	180

2.2.1 History and Rationale for SBRT

Current radiobiological models of cell-kill by ionizing radiation are built upon years of outcome data for conventional fractionation schemes on the order of 30-40 fractions, not large fraction doses delivered in 1-5 fractions. This shift in paradigm is the result of technological advances in image guidance and treatment delivery techniques that enable the delivery of large doses to tumors with reduced margins and sharp dose fall-off outside the target volume. Technologies like TomoTherapy allow physicians to sculpt the dose around critical organs, minimizing the risk of toxicities. Despite an increasing number of cancer patients being treated with SBRT in recent years, the biological mechanisms of SBRT remains unclear. Some evidence suggests that doses higher than 10 Gy per fraction induces severe vascular damages in tumors, which causes secondary tumor cell death (25). The extensive injury and death of tumor cells then induces a release of tumor-specific antigens and elicits an anti-tumor immunity response (26,27).

While the radiobiological mechanism may be unknown, prospective series with mature data have shown promising clinical outcomes that appear superior to those with conventionally fractionated radiotherapy. Recall that surgical resection remains the standard therapy for operable stage I patients. It is associated with a 65% 5-year survival rate. For comparison, the Radiation Therapy Oncology Group (RTOG) conducted a phase II trial to measure outcomes for SBRT (RTOG 0236) that included 44 patients with T1 tumors and 11 patients with T2 tumors (<5 cm). The tumors were required to be greater than 2 cm in all directions from the proximal bronchial tree. Patients were prescribed a dose of 60 Gy in 3 fractions. Updated results of RTOG 0236 showed good primary tumor control was maintained without increase in toxicity. At 5 years, the primary tumor failure rate was estimated to be 7% and the local failure rate was 20%. The 5-year local-regional failure rate was 38% and the 5-year disseminated failure rate was 31%. Five-year disease-free survival was 26% and overall survival was 40% (28). This local failure rate compares favorably to conventional radiotherapy with doses near 60 Gy given in 1.8-2.0 Gy per fraction over 6 weeks, where approximately 60-70% of patients experience local failure and less than 40% are long term survivors (17,18).

There is also evidence suggesting that unlike conventional radiotherapy, SBRT can be used to treat metastatic disease (22). Additionally studies interested in treating oligometastases, a transitional stage of disease between localized and widely metastatic, are investigating if cure is achievable when a certain amount of metastatic sites are eradicated (29). Other studies are exploring the use of SBRT for palliation, particularly when a tumor abuts or overlaps a previously irradiated region (29,30).

Finally, receiving fewer treatments is practically more cost-effective than traditional radiation therapy and more convenient for the patient.

2.3 General SBRT Workflow

A summary of the SBRT workflow at The Queen's Medical Center is presented in this section, followed by a detailed discussion on the challenge of respiratory motion (section 2.4), and a review of the imaging (section 2.5) and treatment (section 2.6) requirements for SBRT.

When a patient is being considered for SBRT, the radiation oncologist will schedule an initial consultation to discuss the treatment options available and their pros and cons. In most cases, the patients have had other diagnostic imaging studies performed that the physician will review to determine if they are eligible for SBRT.

The next critically important step is the SBRT simulation. Immobilization devices are customized to the patient's anatomy to enhance comfort and ensure setup reproducibility throughout treatment. A respiratory monitoring device, called the bellows belt (Philips Medical Systems), is placed around the patient's lower chest to record a waveform of the extent of thoracic/abdominal motion as the patient breathes. A three-dimensional computed tomography (3DCT) scan and a four-dimensional computed tomography (4DCT) scan without abdominal compression are acquired. The 4DCT scan is an oversampled set of 3DCT scans that correlated with the respiratory waveform such that images can be

sorted retrospectively based on the breathing signals. The physician reviews the 4DCT images to assess extent of tumor motion without abdominal compression. Typically, if the maximum tumor displacement is 8-10 mm or more, a second 4DCT scan is acquired with abdominal compression applied to try to reduce the maximum tumor displacement. All images acquired are sent to the treatment planning system. For the next several days following the simulation, the physician, physicist, and dosimetrist designs and optimizes an SBRT plan that delivers the physician-prescribed dose and maintains sufficiently low doses to nearby critical organs ("dose constraints.") When a plan has been selected and approved by the physician, the physicist will check and measure the plan output to ensure the treatment machine delivers the plan correctly. Upon passing this quality assurance testing, the patient is ready to begin treatment.

The first day of treatment is typically the longest, requiring the patient to be set up on the machine with the immobilization devices created during the simulation. Once they are set up on the table, a TomoTherapy MVCT image is acquired to identify the current location of the lung tumor and shift the patient into position. The physician and physicist review and confirm the shifts made, and then the radiation treatment is delivered. The pre-treatment setup and imaging steps are repeated for each subsequent treatment day. Figure 1 shows the imaging steps involved in SBRT. More details surrounding the specific use of TomoTherapy for SBRT are described in Chapter 3.

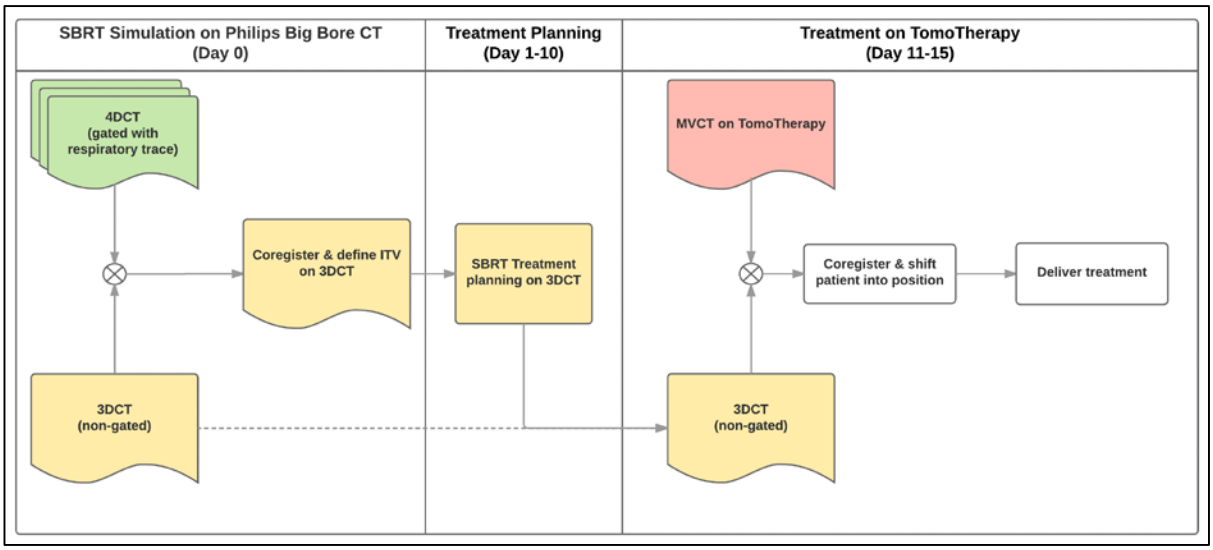

Figure 1. Patient Imaging workflow for SBRT.
The timeframes are approximate and included to clarify the clinical workflow.

2.4 Respiratory Motion

Equipped with the ability to deliver highly conformal doses, one challenge facing SBRT is respiratory motion. The demands of high precision in radiation therapy have led to the development of techniques to control or compensate for breathing-related movement. An overview of the problem breathing poses in SBRT is presented here and recent developments in the management of breathing are briefly explored.

Breathing is a complex process, controlled via the thorax or the abdomen. While breathing is usually cyclic, a typical respiratory cycle may vary considerably over both long and short time periods. Figure 2 illustrates an example of an irregular respiratory waveform recorded during a patient's simulation for SBRT.

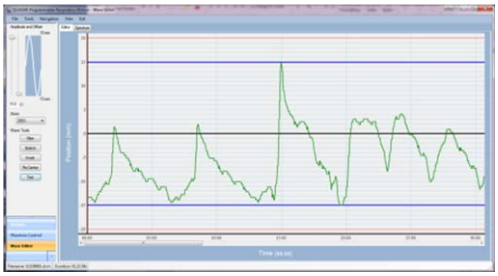

Figure 2. Example of an irregular respiratory waveform recording during a 4DCT simulation

Respiratory motion affects almost all structures in the thorax and abdomen to different degrees depending on the location and surrounding anatomy. For example, tumors located close to the diaphragm (such as in the lower lobes of the lung) and those in the abdomen (such as in the liver) exhibit a greater degree of motion compared to tumors that are attached to the mediastinum, or located in the upper lobes of the lungs. On average, the diaphragm moves approximately 1.5 cm in the superior-inferior (SI) direction during normal breathing. Tumors in the lower lobes of the lung and abdomen move a similar amount. The anterior-posterior (AP) and left-right (LR) motion of both the diaphragm and lung tumors are generally less than the SI motion.

Current techniques to quantify respiratory motion typically involve either real-time tracking of an external marker or surrogate, or direct imaging of the internal anatomy using radiography or CT. One advantage of using a respiratory signal based on external motion is that it is non-invasive, generally requiring neither additional exposure to radiation, nor the implantation of markers in the lung. However, a consistent relationship between external respiratory motion and the internal motion of the tumor is not guaranteed, and thus may affect the accuracy of treatment planning and dose delivery. Studies relating external tracking with internal movement have demonstrated phase offsets that inhibit accurate real-time tracking (31–33). Despite these challenges, externally based respiratory management is more common than direct imaging.

Direct imaging methods provide increased confidence that the true position of the target and/or critical organs is known. For example, to improve radiographic visualization of tumors, radio-opaque markers can be implanted near or within the tumor. This enables the quantification of tumor motion when used with a multiple x-ray tube/detector system that generates simultaneous fluoroscopy recordings from two of four different directions, such as the Brainlab ExacTrac system (Brainlab AG, Munich Germany). However, lung implantation is invasive, and the method exposes the patient to increased imaging dose.

Regardless of the methodology, SBRT requires knowledge of the respiratory motion in order to be administered safely. At the Queen's Medical Center, an external-based respiratory management

approach is used where respiratory waveforms, sometimes called traces, are recorded using the bellows belt.

The bellows belt is a rubber air bellows wrapped around the patient's abdomen and attached to a pressure transducer. As the patient breathes, the abdomen expands and contracts, and the transducer senses air pressure changes within the bellows. This signal is digitized and transmitted to the CT scanner where the respiratory waveform is recorded (34). This waveform is typically divided into 10 equally spaced phases ranging from 0 – 90%, with the 0% phase aligned with full inhalation and the 50% phase with full exhalation. This respiratory trace is stored with the 4DCT images on the CT scanner and can be accessed later if reconstruction using different phases is desired.

To work around the potential asynchrony between the external respiratory signal recorded by the bellows and the actual internal motion of the tumor, a target volume that encompasses the whole range of tumor positions during respiration is defined and used for planning. This is referred to as an ITV, or Internal Target Volume, and will be discussed more in the next section.

2.5 Imaging Requirements for SBRT

The goal of imaging during SBRT simulation is to provide visualization of the patient's anatomy as it will appear during setup and throughout treatment. Treatment planning is concerned with the designation of target(s) and critical structure(s), as well as determining an optimal treatment delivery approach. SBRT requires precise delineation of patient anatomy, targets for planning, and clear visualization during treatment delivery to ensure that the patient is aligned and set up correctly. Because of the delivery of large doses and the impact of respiration, SBRT requires advanced imaging technology to be performed safely. Several methods currently exist, but the most commonly employed method is 4DCT.

Four-dimensional computed tomography (4DCT) involves gathering multiple projections of the same anatomic region at different respiratory phases and then sorting those reconstructed images by phase to create multiple volume reconstructions. Each set of reconstructed images represents a temporal window on the breathing cycle. This sorting is performed by synchronizing the acquisition with the external respiratory waveform generated by the bellows belt and is referred to as phase-based 4DCT. The term "phase" is used to describe a portion of the breathing cycle such as the end of inhalation. This process is not foolproof. Some studies have demonstrated problems with obtaining a reproducible respiratory waveform, resulting in large inconsistencies in the image reconstruction. Vedam *et al.* (31) and Lu *et al.* (35) have shown that amplitude gating is more consistently related to the target position, using tidal volume and air content as a surrogate for an actual tumor.

At the time of 4DCT, the extent of lung tumor motion is evaluated. Because some lung tumors move in excess of 2cm, the ITV can encompass a larger treatment volume than desired. In this case, steps can be taken to reduce the uncertainty of lung tumor location. Patients can hold their breath at a certain respiratory level during the irradiation, or abdominal compression can be applied restrict their

respiratory motion. Another approach is a respiration-gated intermittent irradiation system, where the movements of the skin surface or other physiologic parameters are monitored to coordinate the "beam-on" time with a specific portion of the respiratory cycle. At the Queen's Medical Center, we apply abdominal compression to patients exhibiting respiratory tumor amplitude >1 cm.

2.6 Treatment Requirements for SBRT

SBRT treatments require high conformality, where the shape of the dose fits the shape of the target volume, with sharp dose fall-off outside the target. The American Association of Physicists in Medicine (AAPM) and American Society for Radiation Oncology (ASTRO) publish guidelines for commissioning and implementing an SBRT program (29,36). According to Table 5 in the ASTRO Supplemental Material on safety considerations for SRS (stereotactic radiosurgery) and SBRT, the image guided radiation therapy (IGRT) positioning error should be ≤1 mm, and the end-to-end dosimetric evaluation using an IGRT system (such as TomoTherapy) should be ≤2% (36). This dissertation uses these tolerances to assess the clinical impact of detected imaging and dose discrepancies caused by the interplay effect.

2.6.1 Dosimetry

Radiation therapy is a constraint problem: maximize the dose to the target volume and minimize the dose to surrounding critical structures. We solve this with multiple, non-opposing, non-coplanar beams spread in a large solid angle with fairly equal weighting. This minimizes both entrance and the volume of normal tissue receiving clinically significant radiation. Planning an SBRT case is often an iterative process involving calculations of multiple beam arrangements and scenarios to compare and find a plan that best meets required constraints. Dose constraints used for SBRT are typically based on RTOG guidelines, such as those summarized in Tables 2 and 3.

Table 2. SBRT Dose Constraints for Critical Organs.
Lists the recommended dose and volume limits to critical organs per RTOG 0613 protocol

SBRT Dose Constraints for Critical Structures		
Organ	**Volume**	**Dose (Gy)**
Spinal Cord	Any point	18 Gy
Esophagus	Any point	27 Gy
Ipsilateral Brachial Plexus	Any point	24 Gy
Heart/Pericardium	Any point	30 Gy
Trachea and Ipsilateral Bronchus	Any point	30 Gy
Skin	Any point	24 Gy
Whole lung (right & left)	<10% volume to 20 Gy	

Table 3. SBRT Dose Constraints for Planning Target Volume (PTV)
Lists the conformality and dosimetry requirements for a given length and volume of PTV (RTOG 0813)

Maximum PTV Dimension (cm)	Ratio of Prescription Isodose Volume to the PTV		Ratio of 30 Gy Isodose Volume to the PTV, $R_{30\ Gy}$		Maximum Dose 2 cm from PTV in any Direction, D_{2cm} (Gy)		Percent of Lung receiving 20 Gy total or more, V_{20} (%)		PTV Volume (cc)
	Deviation		Deviation		Deviation		Deviation		
	none	minor	none	minor	none	minor	none	minor	
2.0	<1.2	1.2-1.4	<3.9	3.9-4.1	<28.1	28.1-30.1	<10	0-15	1.8
2.5	<1.2	1.2-1.4	<3.9	3.9-4.1	<28.1	28.1-30.1	<10	10-15	3.8
3.0	<1.2	1.2-1.4	<3.9	3.9-4.1	<28.1	28.1-30.1	<10	10-15	7.4
3.5	<1.2	1.2-1.4	<3.9	3.9-4.1	<28.1	28.1-30.1	<10	10-15	13.2
4.0	<1.2	1.2-1.4	<3.8	3.8-4.0	<30.4	30.4-32.4	<10	10-15	21.9
4.5	<1.2	1.2-1.4	<3.7	3.7-3.9	<32.7	32.7-34.7	<10	10-15	33.8
5.0	<1.2	1.2-1.4	<3.6	3.6-3.8	<35.1	35.1-37.1	<10	10-15	49.6
5.5	<1.2	1.2-1.4	<3.5	3.5-3.7	<37.4	37.4-41.7	<10	10-15	69.9
6.0	<1.2	1.2-1.4	<3.3	3.3-3.5	<39.7	39.7-41.7	<10	10-15	95.1
6.5	<1.2	1.2-1.4	<3.1	3.1-3.3	<42.0	42.0-44.0	<10	10-15	125.8
7.0	<1.2	1.2-1.4	<2.9	2.9-3.1	<44.3	44.3-46.3	<10	10-15	162.6

As mentioned earlier, many centers including The Queen's Medical Center define an ITV as the union of all locations of the tumor during the 4DCT scan. As long as the tumor remains within the ITV boundary, the SBRT treatment plan will deliver the high fraction dose to the tumor.

2.6.2 Treatment Delivery

Once an SBRT plan is designed and approved by the physician, a physicist reviews it and collects measurements to ensure that the treatment delivery system can produce the desired dose distribution. Next, the patient begins his or her treatment. On the first day, the treatment delivery typically takes 1-1.5 hours. It is imperative that the patient is set up on the treatment machine the same way that the 4DCT images were acquired, including any immobilization and abdominal compression devices.

The patient is then imaged using the available imaging system for the treatment unit. These images are coregistered with the simulation CT to determine any necessary fine-tuning shifts. Once the patient is shifted into place, the beam is turned on, and the first dose of radiation is delivered. Compared to conventional radiotherapy, SBRT treatments typically involve significantly more immobilization devices, abdominal compression, and tighter tolerances for determining whether the patient is in the correct location, particularly if there is some variation that requires a judgment between aligning the tumor or keeping a critical organ away from the radiation field. At the Queen's Medical Center, the physician and physicist are required to be present at the treatment console to review and approve the final shifts prior to treatment.

To ensure the large doses of radiation are aimed at the tumor and not at healthy organs, some commercially available systems, such as the Cyberknife (Accuray, Inc., Sunnyvale, CA) or the Brainlab ExacTrac system (Brainlab AG, Munich, Germany) will pause treatments and take images intermittently to

verify the patient remains in the same position. Devices such as the TomoTherapy will divide up the large fraction dose into 2 or 3 “passes” with imaging in-between to confirm the patient has not shifted. Other systems aim to deliver the treatment as quickly as possible based on the theory that the longer the patient lies on the treatment table, the more uncomfortable they will become, increasing the chance for movement.

Chapter 3 Principles of SBRT with TomoTherapy

This chapter provides a brief description of the TomoTherapy system and how it can be used for SBRT. It also provides a brief description of the interplay effect.

3.1 Overview of TomoTherapy

The TomoTherapy Hi-ART is an imaging system integrated with an intensity modulated radiation therapy (IMRT) treatment delivery system. The TomoTherapy system looks like a helical CT scanner with a 6 megavolt (MV) linear accelerator (linac) mounted on a slip ring gantry. The beam traverses a primary collimator and is further collimated into a fan-beam shape by an adjustable jaw. In the superior-inferior, or y-direction, the beam is collimated by an adjustable jaw with three distinct treatment slice widths of 1.0, 2.5, and 5.0 cm at isocenter. For further collimation and beam shaping, a binary multileaf collimator (MLC) is used. The binary MLC has 64 “leaves” that divide the fan beam in the x-direction, and each MLC leaf is either closed or open and intensity modulation is achieved by adjusting how long each leaf is open. The MLC is pneumatically driven and consists of two separate banks, allowing for a rapid transitioning (about 20 ms) of the leaf. The result is a system where the gantry continuously rotates around the patient as the patient is continuously translated in the y-direction through the center of the bore. As the gantry is rotating, the MLC leaves are opening and closing in quick procession to shape the beam that is hitting the patient.

3.1.1 TomoTherapy MVCT Imaging

When a patient begins their course of SBRT on the TomoTherapy system, they are first imaged to determine the shifts necessary to move the patient into position. The imaging system on the TomoTherapy is referred to as MVCT, which stands for megavoltage computed tomography. The reason is that the radiation beam used for imaging on the TomoTherapy unit is generated by the same linac that generates the 6 MV treatment beam. Therefore, the radiation energy is in the megavoltage range. For MVCT imaging, the accelerator is adjusted such that the nominal energy of the incident electron beam is 3.5 MV. The imaging detector array, mounted on the rotating gantry opposite the linac is an arc-shaped CT xenon detector where the standard image matrix size is 512 x 512 pixels and the field-of-view has a diameter of 40 cm. A filtered back-projection algorithm is used for image reconstruction.

On the operator workstation, the therapist selects the scan length and the slice thickness. Three imaging options are available, referred to as fine, normal, and coarse modes, corresponding to pitch values of 1, 2, and 3, and nominal slice thicknesses of 2, 4, and 6 mm, respectively. The rotational period during the image acquisition is fixed at 10 seconds.

Recall that the MVCT registered with the planning CT to determine how to shift the patient to align the tumor where it needs to be. In the case of SBRT for lung tumors, the tumor is constantly moving during MVCT acquisition, leading to imaging artifacts. In addition, due to the helical nature of the MVCT

acquisition, the interplay effect is a potential concern. In Chapter 5, the interplay effect for each of the three MVCT modes is investigated.

3.1.2 TomoTherapy Treatment Delivery

After the patient is shifted into position, the first SBRT fraction can be delivered. Depending on the SBRT fraction dose, the dose may be delivered in 2 or 3 “passes” where each pass delivers 6-7 Gy and takes 5-10 minutes or more, depending on the size of the target volume and whether 1 cm or 2.5 cm slice width is used. After the first pass is completed, a second MVCT scan is performed to ensure the tumor has not moved. If necessary, a shift is made, and then the second pass is given. This is repeated until all passes have been delivered, constituting a single SBRT fraction.

Due to the design of the machine, creation of a TomoTherapy plan requires selecting parameters that do not exist in conventional radiotherapy plans: treatment slice width, pitch, and modulation factor. The treatment slice width is the fan-beam width that is defined by the collimating y-jaws in the longitudinal direction at isocenter, and is selected from either 1.0, 2.5, or 5.0 cm. The pitch is defined as the ratio of the distance traveled by the couch in one gantry rotation to the treatment slice width and it is recommended to be set less than 1. The modulation factor (MF) is defined as the longest leaf opening time divided by the average of all nonzero leaf opening times. The longest leaf opening time is significant because it determines the gantry rotation speed that is used during the delivery. Using the planning software, the user places an upper bound on the modulation factor values available to the optimization software. The final treatment plan may thus have a smaller modulation factor than the user entry. Treatment slice width, pitch and MF all affect plan quality and treatment time. Many studies attempt to optimize the pitch and modulation factor selection for conformality and treatment time (37–42).

The integrated imaging system and ability to generate highly conformal dose distributions make TomoTherapy a reasonable machine for SBRT treatments. Numerous studies have found that TomoTherapy improves dose homogeneity and decreases doses to the organs at risk when compared to conventional linac-based IMRT. In addition, SBRT delivered using TomoTherapy has demonstrated excellent toxicity profile in the treatment of peripheral early-stage NSCLC and lung metastases (9,43–46).

3.2 Interplay Effect

For TomoTherapy treatments where the couch translates into the bore while gantry rotates, breathing induced motion may push the lung tumor into and out of the treatment field and result in dose discrepancies between what is planned and what is actually received by the patient. The result is a strong time dependency of the delivered radiation on the longitudinal location (8,13,47). Importantly, it is possible for the lung tumor to effectively be out of the beam for a significant percentage of time. This is commonly referred to as the “interplay effect.”

Several studies have investigated the interplay effect for TomoTherapy, and all generally conclude that for conventional fractionation treatments, where a patient is treated 20-30 times, the interplay effect likely averages out.

Two early studies performed simplified simulations of the interplay effect using sinusoidal waveforms. Yu *et al.(48)* and *Kissick et al*.(13) both performed a computational simulation of the interplay between a sliding jaw motion and respiratory motion. In both studies, the respiratory motion of the target was a sinusoid, and a slit beam was used to represent the radiation field. Under these conditions, fluence is only accumulated during those times when a given voxel in the target sees the beam. In Kissick's study, additional simulations were performed where some random variation to the amplitude and frequency were introduced to the sinusoidal waveform. Their simulations exposed a "ramping effect" at the ends of the target attributed to moments when the distal edge of the jaw passes over the proximal end of the moving target or when the beam is off before the proximal jaw reaches the distal end of the target. In addition, if the slit beam scanned across the moving target slowly (on the order of 0.1 cm/sec), the moving target would enter and exit the beam many times, such that the variation in intensity is less than the case where the beam scans across quickly. Both studies concluded that the effects would average out over the course of many fractions, but the fluence intensity variation plots for a single fraction were found to be highly variable for both the random amplitude and random frequency oscillations. These simulations did not include the effect of scattered photons, dose transport, or the divergence of the beam.

A study by Yang *et al*.(49) experimentally tested the simulations by Kissick and Yu by constructing a computer-controlled phantom. The phantom was a cylindrical water phantom that consisted of two closed half-cylindrical acrylic shells that could sandwich a sheet of Kodak XV film. The phantom mechanically rotated about the vertical axis, and had a stepper motor that could translate it up and down to mimic respiratory motion. Using a conventional linac with the collimator narrowed to effectively create a slit beam, film exposures were made to investigate the impact of longitudinally cyclic motion, using different cylindrical rotation rates and longitudinal amplitudes and frequencies. The study showed that the longitudinal breath motion extended the dose fall-off at the superior-inferior edges, and that for a 2-cm slit width and rotation at 4 rotations per minute, the relative dose variation was ±5%. Larger variation in dose profiles were found when the 'respiratory' frequency was closest to the beam rotation frequency and as amplitudes increased. Yang also concluded that a conventional treatment of greater than 20 fractions would smooth out any overdosed or underdosed areas assuming the phase difference between the rotating radiation field and the longitudinal cyclic motion of the target was randomly distributed.

Chaudhari *et al*.(47) built upon the work of Yu and Kissick by running a simulation of a simple unmodulated beam, modeled using measured beam profiles instead of fluence, that incorporated respiratory waveforms from 52 patients. The respiratory data incorporated tidal volume measurements via spirometry and the external displacement signal using a bellows device. Tumor motion was then simulated using a variable scale factor multiplied by the tidal volume data for each patient, and

normalized to 0 to 2-cm. Their investigation evaluated the impact of field width (1-cm or 2.5-cm), couch speed, and breathing amplitudes, where breathing amplitudes were defined as the motion corresponding to the 80th percentile in tidal volume. They proposed a dose-error ratio metric, which is the ratio of the dose with motion to the dose without motion, calculated along the central axis of a simple cylindrical volume along the TomoTherapy axis of rotation. The calculated dose profile was convolved with the simulated motion and compared with the dose profile without motion. Calculated results were tested for a single patient, using an in-house motion phantom and radiochromic film, though the conventional fraction dose was not specified.

Results showed blurring on the superior-inferior borders as expected. For the 1-cm jaws, they measured larger dose-error ratios regardless of the breathing motion amplitudes, exceeding 10% even with amplitudes of 0.5-cm. For the 2.5-cm jaws, the dose-error ratios were smaller, though dose errors greater than 10% were observed with breathing motion amplitudes of 1-cm or more. They also observed that the dose-error ratio increased until the motion was greater than the corresponding jaw-width, as well as with increasing pitch values, and suggested use of a larger field width and slower couch velocities to minimize the motion-induced errors.

One limitation to this study is the use of a scaling factor and tidal volume to simulate tumor motion. Several studies have observed that external surrogates are not necessarily representative of the internal motion of a lung tumor (33,50,51). Second, for the film measurement, the couch velocity was incorporated into the model instead of having the film irradiated with the couch moving. Chaudhari *et al.* also proposed that subtle drifts in the exhalation position may lead to increased dose-errors, however, it is unclear how baseline shifts in the respiratory signal would correlate with changes in tumor position for an actual patient.

Another study by Kanagaki *et al*.(52) involved the use of a motion platform they designed, upon which a heterogeneity lung phantom was placed to simulate a lung tumor patient. A 3-cm spherical putty ball represented the tumor and was contoured as the clinical target volume (CTV) on CT without any additional margin. Six TomoTherapy plans were designed, two plans used the 1-cm jaw and four plans used the 2.5-cm jaws, and all used a pitch of 0.3 to deliver doses of 2 Gy to 95% of the CTV. The phantom was programed to move with peak-to-peak amplitudes of 1.2 cm and 2 cm with either a 3-sec or 5-sec breathing period. Kodak EDR2 film was irradiated 30 times to simulate a conventional 30-fraction treatment course. Kanagaki found overdosage of 110-120% within the CTV with a corresponding decrease in the volume of lung receiving 20% of the prescription dose (V20) by an average of 16.7%. Cold spots were observed on the superior-inferior borders of the films treated with the 1-cm jaw plans, leading to a significant reduction in CTV coverage from 95% volume coverage down to 78%. The authors concluded that the 2.5-cm jaw plans were less susceptible to motion effects than the 1-cm jaws. Contrary to Yang's assertion above, however, Kanagaki achieved better dose distribution agreements when the gantry rotation time was closer to the phantom moving period. Ultimately, they concluded that they did not observe any interplay effects.

While this study delivered actual TomoTherapy plans to a heterogeneous phantom, there were some limitations. The details regarding the cyclic motion of the platform were not described fully in the manuscript, so it can only be assumed that the motion was sinusoidal. In addition, the platform moved the entire lung phantom in the superior-inferior direction, as opposed to just the lung tumor, which may be why significant interplay effects were not seen. In true respiration, the external body of the patient remains relatively stationary (with the exception of the anterior border of the abdomen and thorax moving with respiration), and it is primarily the lung tumor that is moving internally.

Another study using computer modeling and film-based verification with a motion phantom was performed by Kim *et al.* who investigated the impact of the amplitude of target motion and the periodicity of the motion on three types of motion-induced dose discrepancies. They theorized the interplay effect was comprised of three components: dose rounding, dose rippling, and the "IMRT leaf opening asynchronization" effect (53). Dose rounding refers to the spreading of the penumbra of the delivered dose near the edges of the target volume along the direction of the tumor motion. Simulating a non-IMRT plan and validating with film measurements, the dose rounding effect was found to worsen with increasing target motion amplitude. In addition, when the target motion period was 8 seconds, a smaller penumbra size was observed. Dose rippling refers to the bands of overdose and underdose within the target region along the direction of couch motion. This effect was attributed to the asynchronous interplay between the couch motion and the longitudinal tumor motion with a fixed frequency, and a dose rippling parameter (β) was introduced as the ratio of the time required for the couch to travel the distance of one jaw width to the target motion period.

(3) $$\beta = \frac{T_g}{p\,T_r}$$

where T_g is the gantry period (rotations per second), p is the pitch, and T_r is the respiratory period (breaths per second). When β was an integer, it was characterized as synchronous interplay such that there would be an absence of dose rippling, and as β increased above the value of 4.5, the magnitude of rippling would become less significant. The IMRT leaf opening asynchronization effect described the interplay between the timing of the leaf openings and longitudinal motion of the target volume, and was prominent in the example IMRT case, where the difference between the stationary and motion dose profiles ranged from -29% to 7%. To estimate the effect over 30 fractions, the starting phase of target motion was randomly selected for each fraction and the calculated dose profiles were summed. Compared to the static profile, the composite random motion phase profile had differences that ranged from -16.5% to 1.5%. This seems to suggest that multiple fractions may not necessarily average out the dose discrepancies, unlike earlier simplified simulations suggested.

This computer simulation model developed by Kim *et al*. offered a compelling characterization of the different types of interplay effect, although only results for the 2.5-cm jaw width plan were presented. Additionally, the introduction of a dose rippling parameter offers a framework for evaluating the potential

for the dose rippling effect, though pitch and gantry period are not directly selectable in the TomoTherapy system, and are intertwined along with the modulation factor. As a planning guide, it may not be practically useful until after an optimized plan has be developed. Regarding the IMRT leaf opening asynchronization effect, Kim asserted that some form of gated TomoTherapy delivery would offer the best solution for minimizing this effect. Unfortunately, such an option remains currently unavailable for clinical use.

A study by Klein *et al.(14)* evaluated the interplay effect using the ArcCheck phantom (Sun Nuclear, Melbourne, FL) which is a cylindrical phantom with 1,386 diode detectors around the other surface. The ArcCheck was placed on a programmable motion platform and simulated. A CTV and organs-at-risk were contoured on the images and used to create 9 TomoTherapy plans, with different pitches, modulation factors, and all 3 jaw widths. Each plan was designed to deliver 4 Gy to the CTV. Sinusoidal waveforms and 1 respiratory waveform from an actual patient were used to program the platform. Results indicated that the largest dose discrepancies occurred with the 1-cm field width and larger motion amplitudes. Referencing the study by Kim *et al.*, the authors reported observing dose rounding for all measurements, but no dose rippling nor leaf-opening asynchronization effect.

One reason Klein *et al.* did not observe the dose rippling nor the leaf asynchronization effects may be how the ArcCheck was moved using a motion platform. With a motion platform, similar to the one used by Kanagaki *et* al.(52), the entire ArcCheck device is moving according to the respiratory pattern rather than just an internal component such as with the Quasar motion phantom used in the study by Kim *et al*.(53) Moving an entire phantom during radiation will result in the dose blurring effect, which is indeed what was seen, but the dose rippling and leaf asynchronization effect is more evident with a relatively small internally moving target volume residing within a stationary larger outer body.

Using a research version of a MATLAB (Mathworks, Natick) script called CheckTomo, Tudor *et al.(8)* simulated the effect of the respiratory waveforms on a given TomoTherapy plan. Seven respiratory waveforms from patients were decomposed into two components referred to as the baseline shift trace and the cyclic trace. These traces were used to program a moveable platform that moved a water-equivalent cylindrical “Cheese” phantom with a PTV and organ-at-risk structures. Ten plans of different field width, pitch, and modulation factors were designed to deliver a dose of 2 Gy per fraction to the Cheese phantom. Validation of the simulations were performed using GafChromic EBT film sandwiched between the two hemispheres of the Cheese phantom.

The resulting simulations suggested that the interplay effect is largely due to the baseline shift component of the respiratory waveforms. However, this baseline shift was determined by evaluating the relative amplitude of peak-exhalation points on the respiratory waveforms, which are based on the real-time position of a box with optical reflectors placed on the xiphisternum. As the patient breathes, the xiphisternum moves anteriorly-posteriorly, and this motion is detected by an optical camera mounted on the ceiling. It was not demonstrated that the baseline shift of the respiratory waveform translated to a baseline shift of the internal tumor. A second limitation, which the other authors pointed out, is that the

CheckTomo simulation applies the respiratory motion to the patient as a whole, as opposed to the relative motion between an internal target and a stationary outer body.

The interplay effect for TomoTherapy has been studied using simplified models such as regularly shaped breathing traces (13,48,49,52,53) or unmodulated beam delivery (13,47–49). These studies suggest that fractionation tends to average out the hot and cold spots within the target. Three studies incorporated patient respiratory waveforms but all used motion platforms to move phantoms in their entirety, and did not explicitly look at SBRT-type doses (8,14,47).

In the case of SBRT treatments, the interplay effect could adversely impact treatment effectiveness in two ways: 1) reduce the imaging accuracy for tumor localization prior to treatment, and 2) reduce the dose actually delivered to the tumor. This dissertation investigates the interplay effect specifically in the context of SBRT, using a cohort of patient respiratory traces, using a phantom that simulates internal tumor movement, and evaluates the interplay effect of both TomoTherapy's MVCT and SBRT dose delivery.

Chapter 4. Characterization of Respiratory Waveforms

4.1 Introduction

An investigation of the interplay effect for SBRT first requires a closer look at the respiratory waveforms of these patients. Most patients do not breathe in a perfectly sinusoidal pattern, and instead breathe with varying amplitudes, frequencies, sharp and shallow peaks and valleys, with generally longer exhales, and shorter inhales (50,51,54). For this project, I examined the respiratory waveforms of SBRT patients that were recorded with a bellows belt at the time the patient underwent a 4DCT study. While this waveform represents the external abdominal motion during breathing, it does not represent the internal motion of the tumor. The tumor positional information could only be derived from direct examination of the 4DCT images.

In this chapter, I describe how I created an estimate of lung tumor motion during the 4DCT acquisition for each case. It is important to note that this process assumes a constant phase relationship between external and internal tumor motion, which is not necessarily true. However, for the purposes of investigating the interplay effect using an ITV-based treatment, this assumption is acceptable. This process serves as the basis for further analysis and evaluation of the interplay effect described in later chapters.

4.2 Methods

The images and respiratory traces of patients who received a 4DCT simulation and were treated with SBRT on the TomoTherapy system were collected. Actual tumor displacement (“amplitude”) during respiration was measured using the patients’ images, and the respiratory waveforms were modified to program a phantom with a movable plastic tumor insert. In this way, the phantom simulated the actual motion of a patient’s lung tumor during respiration.

4.2.1 Patient selection

Between 2010 and 2015, 62 lung cancer patients in the Department of Radiation Oncology at The Queen’s Medical Center (QMC) were treated with SBRT using Tomotherapy (Accuray Inc., Sunnyvale, CA). Departmental protocol stipulated all SBRT patients undergo a 4DCT simulation on the department’s Philips Brilliance Big Bore 16-slice CT scanner (Philips Medical Systems, Cleveland, OH). Of these 62 patients, the department retained the images and respiratory waveforms of 25 patients in the scanner archives. One patient was excluded due to the acute irregularity of the respiratory pattern such that the phantom could not accurately follow the trace. Two additional patients were excluded due to having such small tumor displacements (less than 1 mm) such that the CT scanner was unable to resolve the peaks from the troughs during a 4DCT simulation of the phantom. The final cohort of 22 patients consisted of 16 males and 6 females, with a median age of 78.5 years old (range 59 – 96). Of these 22 patients, 10 patients had more than 1 set of 4DCT images. The result is a compilation of 35 distinct 4DCT images with

corresponding respiratory waveforms (Table 4). Copies of each of these studies and the corresponding respiratory waveforms were de-identified and assigned a case number, such that the original patients' images remained untouched.

Table 4. Patient Demographics of SBRT Cohort

Patient Demographic Profile	
	Patients N=22
Sex	
Male	16
Female	6
Age, yrs	
Median	78.5
Range	59 – 96
Location of Lung Tumor	
Upper lobe, left	4
Upper lobe, right	5
Mid lobe, left	0
Mid lobe, right	5
Lower lobe, left	4
Lower lobe, right	4
Compression	
No compression	21
With compression	10

4.2.2 Maximum Tumor Displacement

The 4DCT image studies and respiratory traces were transferred to a contouring workstation (MIM Maestro, MIM Software) and reviewed. On each phase of the 4DCT study, the visible lung tumor was auto-contoured using the region-grow tool with preset of -476/73. The centroid coordinates of the tumor on each phase were used to estimate the extent of maximum tumor displacement during the observed respiratory cycle using principal component analysis (PCA). The value of maximum tumor displacement was then used to define the amplitude of the respiratory waveform.

4.2.3 Respiratory Waveform

Before the respiratory waveform could be used to program the motion phantom, some modifications needed to be applied. First, because the 4DCT image acquisition is typically completed within 1-2 minutes, the respiratory trace recorded by the scanner is only 1-2 minutes long. An SBRT treatment on TomoTherapy, however, can take up to 10 minutes per pass (excluding imaging time), requiring that the motion phantom be programmed for at least 10 minutes to complete proper data

acquisition described later in Chapter 5. This required looping the recorded respiratory trace. Second, the amplitude of the respiratory waveform determines how far to displace the plastic tumor. Patients rarely breathe with the exact same diaphragm displacement in each breath, so the respiratory waveforms possess both variable amplitudes and a low-frequency component. The amplitude needed to be normalized so that the phantom would reproduce the actual tumor displacement measured with 4DCT.

4.2.4 Motion Phantom

The Quasar Respiratory Motion Phantom (Modus Medical Devices Inc., London, ON, Canada) is a device that moves a cylindrical insert in the superior-inferior direction and can be programmed to follow any arbitrary motion pattern with a variable speed (range of 4-60 cycles per minute) and amplitude (range of 0-40 mm peak-to-peak). The cylindrical insert used in this portion of the study is 8-cm in diameter, 18-cm long, and composed primarily of cedar (0.4 g/cm^3) to simulate the density of lung. Embedded in the insert is a 3-cm diameter plastic sphere that simulates a tumor ("plastic tumor"). Once the respiratory waveforms were adjusted such that the amplitudes matched the maximum tumor displacement, they were loaded into the Quasar Motion Management software that controlled the motion phantom.

4.2.4 Process Validation

To validate the method used to program the phantom, some preliminary investigation was performed. A simple sinusoidal motion pattern was uploaded to the phantom with a frequency of 15 bpm and a peak-to-peak amplitude of 2.0 cm. The bellows device was wrapped around the phantom and a 10-phase 4DCT scan was acquired on the Philips Big Bore CT scanner (Philips Medical Systems). On the 4DCT images, the plastic tumor was outlined and the centroid locations were calculated for each of the 10 phases. Using principal component analysis (PCA), the maximum tumor displacement was calculated and found to be 2.0 cm, demonstrating the phantom's accurate reproduction of the uploaded motion waveform (Table 5).

Table 5. Preliminary PCA Analysis of Tumor Motion

Preliminary PCA Analysis of Tumor Motion

Respiratory Phase of Plastic Tumor	PCA (cm)	Peak-to-Peak Amplitude based on PCA (cm)	Programmed tumor displacement (cm)
0%	-0.98	2.03	2.00
10%	-0.84		
20%	-0.40		
30%	0.22		
40%	0.82		
50%	1.04		
60%	0.88		
70%	0.34		
80%	-0.30		
90%	-0.78		

To validate the normalization of the respiratory waveforms, an end-to-end 4DCT study of the motion phantom was performed for each patient respiratory waveform used (n=35). The motion phantom was programmed to move with the normalized respiratory waveform with amplitude set to the maximum tumor displacement for that patient, and a 4DCT study was conducted. The plastic tumor was auto-contoured and centroid coordinates extracted. Maximum displacement of the plastic tumor was determined using the same PCA process and compared with the actual patient's tumor displacement to confirm they were the same.

4.3. Results

4.3.1 Visual Review

Across the range of the 35 respiratory patterns that were analyzed, most patient respiratory patterns varied throughout the 4DCT acquisition. A review of the respiratory patterns shows that for all 22 patients, there were irregular fluctuations in the respiratory pattern during the 4DCT acquisition. No patient demonstrated perfectly regular breathing. Figure 3 illustrates a few examples of patient respiratory waveforms.

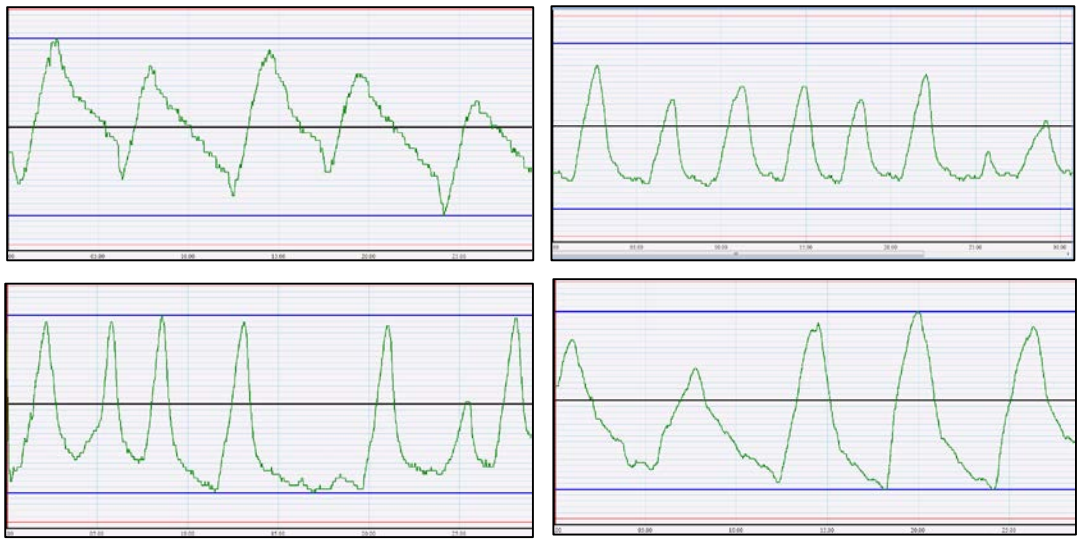

Figure 3. Sample Respiratory Waveforms
(clockwise from top-left: Case 6, 8, 11, 19)

4.3.2 Characteristics of Patient Respiratory Patterns

Among these 35 4DCT studies, the median average breath frequency was 17 breaths per minute (bpm), ranging from 8 to 23 bpm. The instantaneous minimum and maximum breath frequencies observed ranged from 4 bpm to 35 bpm. The median tumor amplitude was 0.7 cm, ranging from 0.2 cm to 2.1 cm. The characteristics of the 35 4DCT studies are summarized in Table 6.

Table 6. Characteristics of Respiratory Waveforms.

Characteristics of Respiratory Motion	
	4DCT studies N=35
Breath frequency, bpm	
Median	17
Range	8-23
< 15 bpm	6
15-19 bpm	20
> 20 bpm	9
Tumor amplitude, cm	
Median	0.7
Range	0.2-2.1
< 0.6 cm	14
0.6-1.0 cm	10
> 1.0 cm	11

4.3.3 Effect of Compression

Ten patients in the cohort received more than one 4DCT scan due to the need for abdominal compression, and 8 of them showed an increase in breath frequency. In one patient, the breath frequency decreased by 1 bpm, and in another patient, there was no measurable change in the average bpm recorded during the 4DCT acquisition. Paired-samples t-test indicated application of compression correlated with increase of breath frequencies (*t(9)=2.36, p=0.04*) by 1.5 bpm.

4.4 Discussion

While a typical 4DCT acquisition is around 1-2 minutes long, an entire SBRT session requiring 3 passes could lead to an overall treatment time of 1 hour. By extension, during a 1 hour treatment time, the patients' respiratory pattern would likely fluctuate considerably (33), and it is unlikely for a patient to breathe identically during simulation and treatment. If an ITV-based approach is not used, the ability to internally track the tumor location at the time of treatment is necessary, and reliance on external respiratory signals should be avoided.

The application of compression appears to result in faster breathing frequencies, despite the small sample size (n=10). This is a key point to note, since in subsequent chapters, it is determined that slower breath frequencies appear to enhance the interplay effect. Thus, applying abdominal compression may not only reduce the amount of tumor displacement by forcing shallower breaths, it will also increase the breath frequency reducing the impact of the interplay effect.

One limitation of this study stems from the lung tumor contours used to extract centroid data. While an auto-contouring method was applied, using a fixed window and level setting, some patient tumor volumes were sufficiently small that a slight change in contour could significantly alter the coordinates of the tumor centroid. This introduces an uncertainty in determining the tumor amplitude using PCA based on the centroid coordinates. To address this, the 4DCT images were reviewed in cine mode and visual confirmation of the PCA results were conducted.

Another limitation to this study is the assumption that there is a fixed correlation between the respiratory waveform and internal tumor motion. There is currently no available technology at the TomoTherapy unit to track the tumor location in real-time. However, for the purposes of this dissertation, the characterization of the interplay effect is based on comparing the motion condition against the stationary condition.

4.5 Chapter Summary

For the majority of the cases reviewed for this study, the proposed technique for programming a motion phantom was effective at simulating the lung tumor's trajectory. There was overall good validation when comparing the 4DCT of the patient images and the 4DCT of the motion phantom. Performing an end-to-end 4DCT of the normalized respiratory waveform with the PCA-determined tumor displacement for each of the 35 waveforms provided confidence that the motion phantom was sufficiently mimicking the

patient's tumor motion captured at the time of 4DCT acquisition. While there are inherent concerns with using phase-based 4DCT images for gated SBRT treatments, the method proposed herein is sufficient for ITV-based SBRT treatments.

Chapter 5. Interplay Effect: TomoTherapy MVCT

5.1 Introduction

This section of the dissertation investigates the interplay effect for the TomoTherapy MVCT imaging system. My hypothesis is that a moving tumor with higher breath frequencies and tumor amplitudes would lead to larger positional errors compared to the stationary (baseline) condition.

While the ITV theoretically accounts for uncertainties in the size, shape and position of the moving tumor, verification of patient setup relies on the accuracy of the MVCT. If the tumor on the MVCT is 2-mm superior to the ITV, the clinical team will likely shift the patient to align the tumor with the center of the ITV. The question is whether this 2-mm shift is due to the timing of the MVCT acquisition with the moving tumor (ie. interplay effect), or whether it is a true shift in the tumor position that should be corrected.

This phantom study tests the ability of the MVCT system to image a moving target using the cohort of patient respiratory waveforms and tumor displacements that were characterized in Chapter 4. To evaluate the error, an MVCT of the stationary phantom is captured and used as the baseline image against which the motion images are compared. Because the MVCT can be acquired in 3 different modes, each mode is investigated to determine if one mode performs better or worse than the others for moving targets. Results are evaluated for statistical significance using R (R Core Team 2016, https://www.R-project.org/) and for clinical implication using the ASTRO recommended tolerance of <1mm for SBRT imaging systems (31).

5.2 Methods

The Quasar motion phantom was programmed to move an insert containing a plastic tumor ($tumor_{plastic}$) using the respiratory waveforms and tumor amplitudes that were characterized and validated as described in Chapter 4.

To assess the accuracy of the MVCT acquisition of a moving target, the phantom was scanned a total of 6 times per respiratory waveform. First, three MVCT scans were acquired with the $tumor_{plastic}$ stationary and at its central position: one in fine mode, one in normal mode, and one in coarse mode. These scans represent the baseline images against which the MVCT images of the moving $tumor_{plastic}$ are compared. The phantom was then programmed to move the $tumor_{plastic}$ according to the respiratory waveform, looped to repeat so that the $tumor_{plastic}$ did not stop moving during the MVCT acquisition, with the peak-to-peak amplitude set to the patient's maximum tumor displacement. Three more MVCTs were acquired: one in fine mode, one in normal mode, and one in coarse mode. All images were transferred to the MIM contouring workstation for evaluation.

To determine whether the accuracy of the MVCT images was impacted by a reduction in breath frequency, another set of three MVCT scans were acquired (in fine, normal, and coarse modes) using the

same respiratory patterns, but expanded to approximate an average slow breath frequency of 5 bpm. Figure 4 illustrates an example of a waveform that was expanded to 5-bpm.

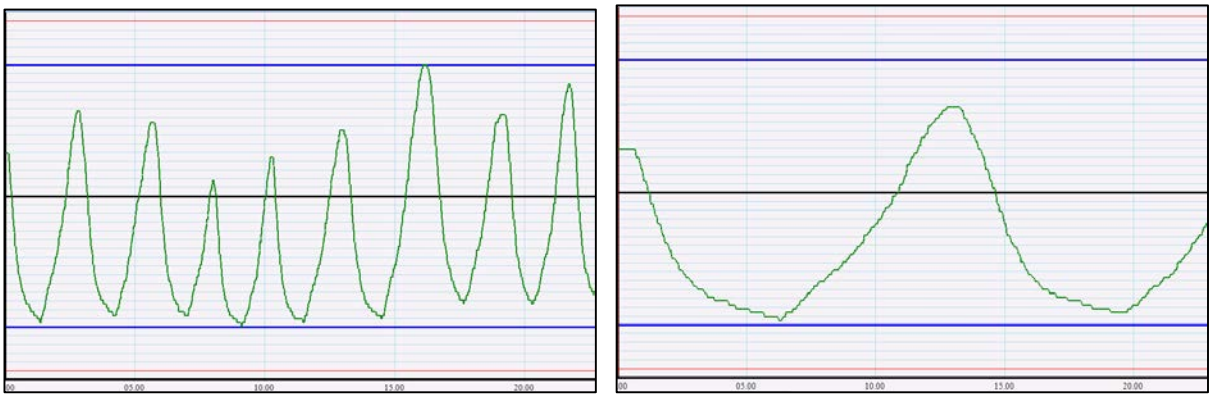

Figure 4. Respiratory Waveform with Native Breath Frequency (left) and Slowed to 5-bpm (right)

In MIM, all 9 MVCTs were loaded. For each mode, the stationary images were coregistered with the images of the moving $tumor_{plastic}$ (native breath frequency and 5 bpm). The $tumor_{plastic}$ on each image was auto-contoured using a preset lung tumor-defined window-and-level setting and the centroid coordinates and volumes were recorded and compared.

5.3 Results

Table 7 summarizes the differences in the X-Y-Z-position (right-left, anterior-posterior, superior-inferior) between the stationary and moving $tumor_{plastic}$ centroids captured for each MVCT mode. The shifts represent the positional error due to motion. Regardless of mode, there was an overall negative-Z (inferior) shift. Inferior shifts were observed in 28 MVCTs in the fine mode, 34 MVCTs in the normal mode, and 29 MVCTs in the coarse mode, and there was an inferior shift for 22 respiratory waveforms in all three modes. A paired-samples t-test was conducted to compare the Z-coordinate of the stationary and moving $tumor_{plastic}$ centroid for each MVCT mode, and significant differences were found in all three modes (Table 7). No correlation was observed between shifts in centroid position and tumor amplitude or breath frequency.

Table 7. Positional Differences for All MVCT Modes.
Difference between centroid positions of the stationary and moving $tumor_{plastic}$ where +ΔX is a shift left, +ΔY is a shift anterior, +ΔZ is shift superior

Positional Differences for All Modes									
	Fine			Normal			Coarse		
cm	ΔX	ΔY	ΔZ	ΔX	ΔY	ΔZ	ΔX	ΔY	ΔZ
Average (SD)	-0.01 ±0.01	-0.00 ±0.02	-0.06 ±0.07	-0.00 ±0.01	0.00 ±0.04	-0.11 ±0.12	-0.01 ±0.02	-0.00 ±0.02	-0.11 ±0.13
$Max_{negative}$	-0.04	-0.04	-0.21	-0.04	-0.19	-0.45	-0.09	-0.04	-0.57
$Max_{positive}$	0.03	0.06	0.08	0.02	0.05	0.06	0.03	0.04	0.08
p-value	0.01	0.84	<0.001	0.10	0.97	<0.001	0.12	0.45	<0.001

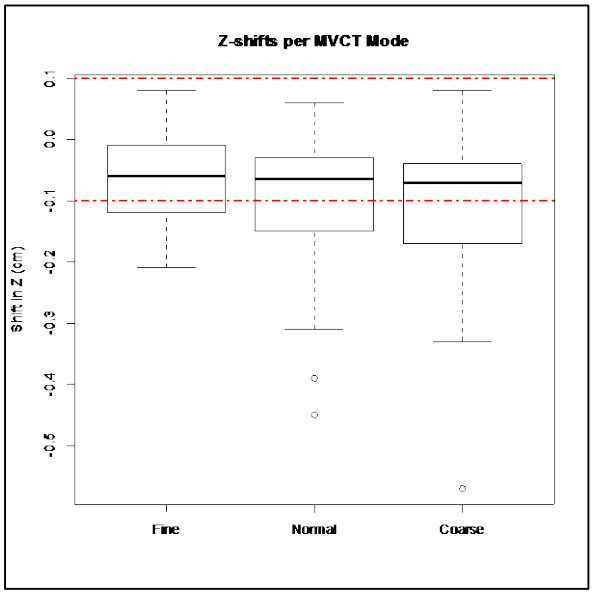

Figure 5. Z-shift in Tumor Centroid.
Difference in Z-position of tumor$_{plastic}$ centroid between the stationary and moving conditions for Fine, Normal, and Coarse MVCT modes; Dotted red line indicates the ASTRO recommended tolerance for SBRT Imaging of ±0.1 cm

When comparing volume measurements, the measured volume of the tumor$_{plastic}$ was generally larger on the motion MVCTs than the stationary scans (Figure 6). Of 35 respiratory patterns, an increase in volume was observed for 32 in fine mode, 34 in normal mode, and 28 in coarse mode. A paired-samples t-test was conducted to compare the volume of the tumor$_{plastic}$ between the stationary and moving conditions; significant differences were found for all modes (Table 8). Note the large volume outlier points on the fine and coarse modes which both belong to the same case (Case 6). Figure 6 (right) represents the volume differences with the outliers removed.

Table 8. Volume Differences for All Modes between Stationary and Motion Conditions

Volume Differences for All Modes			
cc	Fine	Normal	Coarse
Average (SD)	1.63 ±2.95	1.43 ±1.74	1.29 ±3.04
Min	-0.44	-0.25	-0.52
Max	16.25	6.62	17.48
p-value	0.002	<0.001	0.019

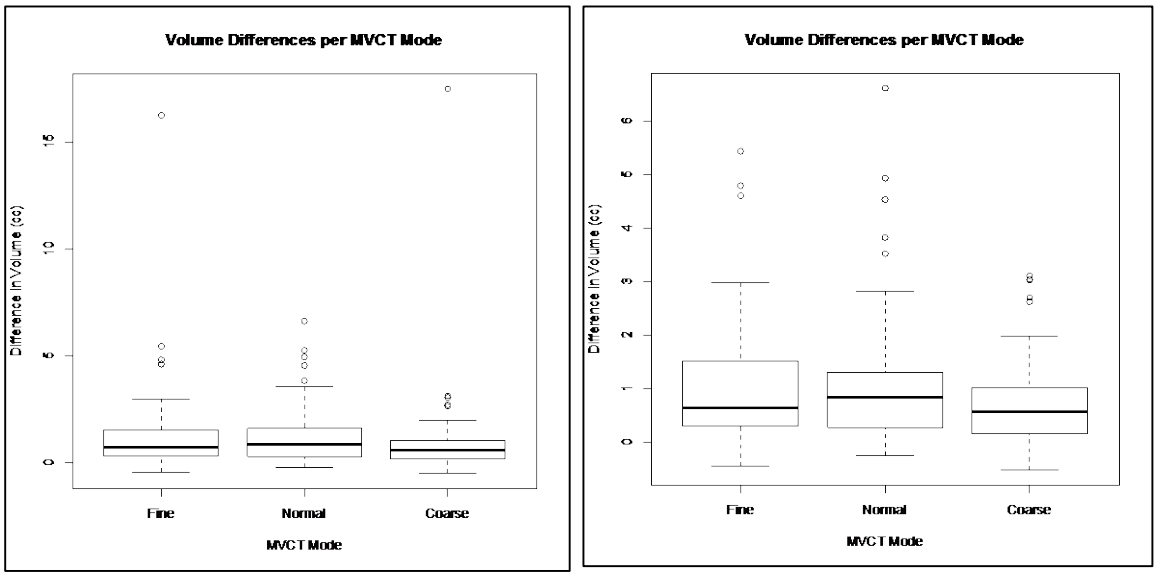

Figure 6. Volume Differences on MVCT. (Left-with outlier; Right-without outlier)

5.3.1 Impact of Tumor Amplitude on MVCT Accuracy

To compare data between cases of low vs high amplitude, 0.6 cm was selected as the cutoff criteria. The rationale for this stratification is that in our clinical practice, tumor displacements on the order of 0.5 cm (estimated by visual inspection) have been considered acceptable for SBRT without compression. This was rounded up to 0.6 cm to include cases where the tumor amplitude was between 0.5-0.6 cm in the "low" group. An independent-samples t-test was conducted to compare the centroid positions with $tumor_{plastic}$ stationary and in motion for each mode (Figure 7). No significant differences were found between low and high amplitude groups in the X- or Y-shifts for all MVCT mode. A significant difference was found for the Z-shifts between the low and high amplitude groups on normal MVCT only ($p = 0.004$). The high amplitude cases had a larger average inferior shift (-0.15 cm) compared to the low amplitude cases (-0.05 cm.)

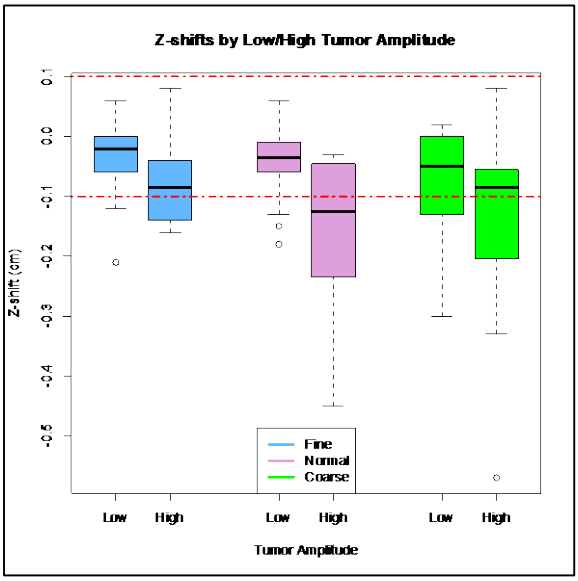

Figure 7. Z-shifts by Low/High Tumor$_{plastic}$ Amplitude;
Dotted red line indicates the ASTRO recommended tolerance for SBRT Imaging of ±0.1 cm

There was moderate to strong correlation between tumor amplitude and volume differences between the MVCTs with the tumor in motion and the tumor stationary as shown in Figure 8. Pearson's correlation coefficients were 0.786, 0.739, and 0.672 for fine, normal, and coarse modes, with fine MVCT showing the strongest correlation.

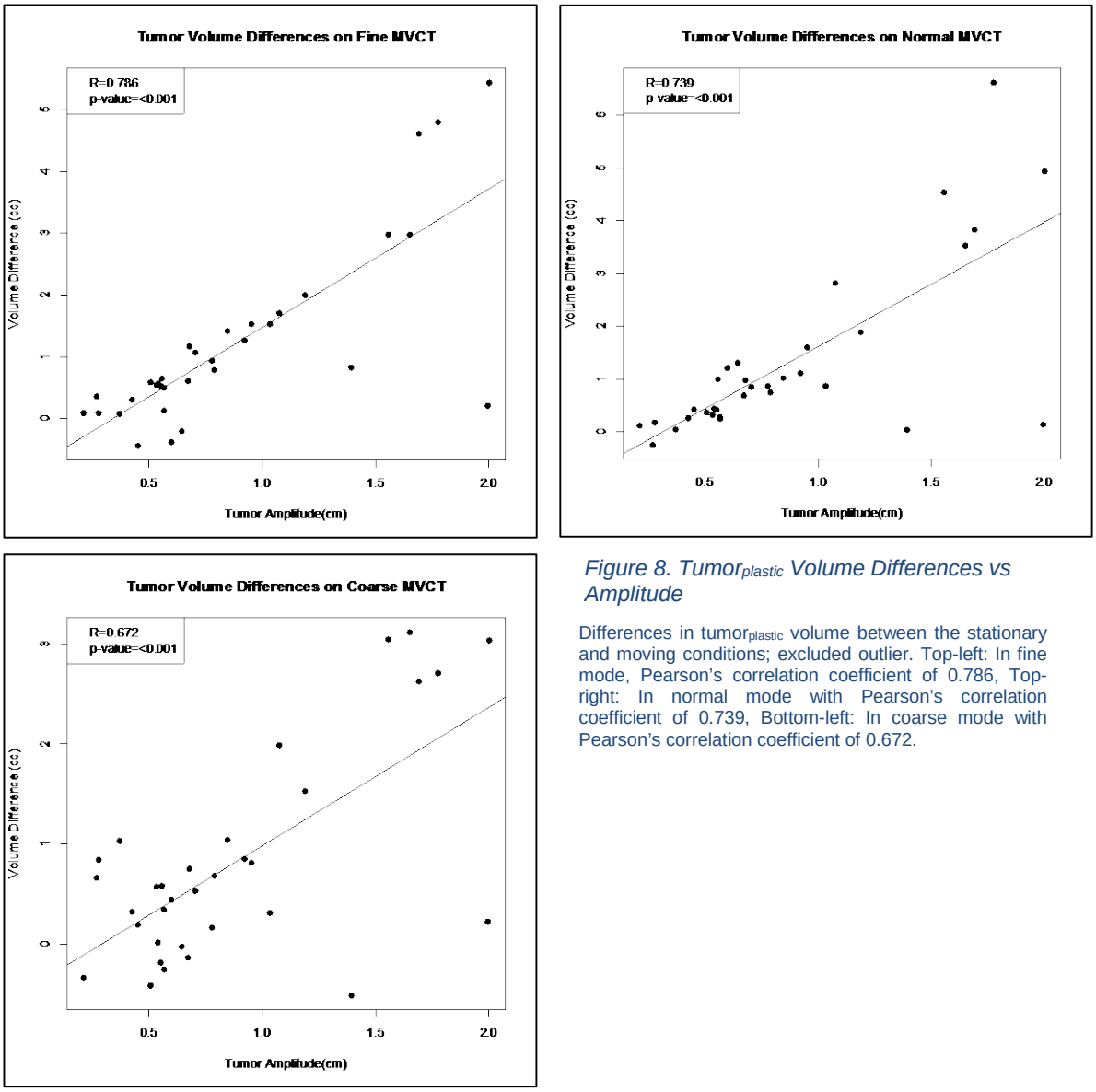

Figure 8. Tumor$_{plastic}$ Volume Differences vs Amplitude

Differences in tumor$_{plastic}$ volume between the stationary and moving conditions; excluded outlier. Top-left: In fine mode, Pearson's correlation coefficient of 0.786, Top-right: In normal mode with Pearson's correlation coefficient of 0.739, Bottom-left: In coarse mode with Pearson's correlation coefficient of 0.672.

When volume differences were stratified by low and high amplitude, there were significant differences for fine (*t=2.91, p=0.01*) and normal (*t=4.12, p<0.001*) modes, but not for coarse (*t=2.02, p=0.06*). The low amplitude group showed an average volume increase of 0.259 cc in fine, 0.362 cc in normal, and 0.269 cc in coarse modes, while the high amplitude group showed much larger volume differences: 2.597 cc in fine, 2.183 cc in normal, and 2.011 cc in coarse modes (Figure 9).

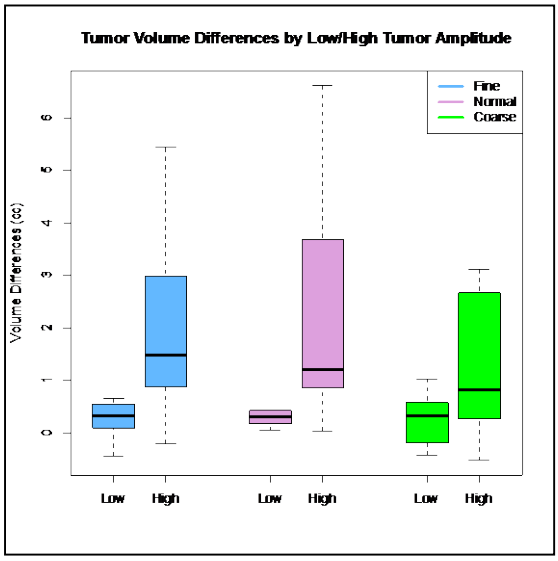

Figure 9. Tumor Volume Differences by Low/High Tumor Amplitude

5.3.2 Impact of Breath Frequencies on MVCT Accuracy

Positional shifts or volume differences do not appear to be influenced by breath frequencies across the cohort (Figure 10.)

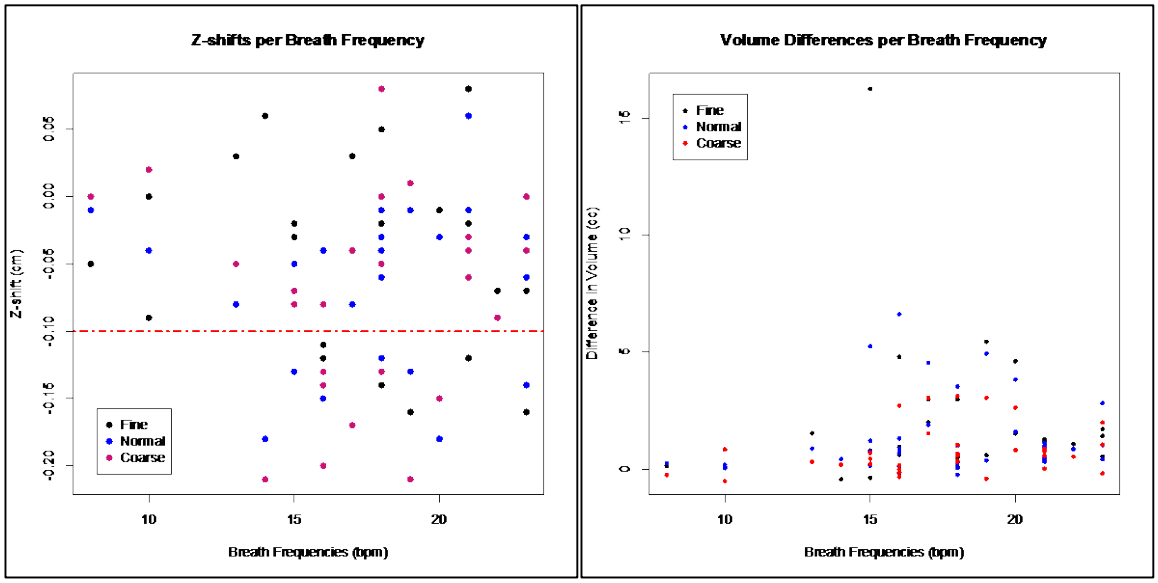

Figure 10. Z-shifts (left) and Volume Differences (right) per Breath Frequency.
Dotted red line on left indicates the recommended ASTRO tolerance of ± 0.1cm.

5.3.3 Impact of slow breath frequency per respiratory pattern

When the respiratory waveforms were reduced to 5-bpm, a paired-samples t-test was conducted to compare the positional shifts for each waveform at the native breath frequency vs at 5-bpm. No

significant difference in positional shifts were found for X- and Y- shifts in all modes. However, a significant difference was observed in the Z-shifts for normal mode where the native bpm shifts were 0.06 cm more inferior than the 5-bpm (*paired-samples t-test, t=-2.46, p=0.02)*.

With tumor volume differences, a paired-samples t-test was conducted to compare the volume difference for each waveform at the native breath frequency vs at 5-bpm. There was no significant difference in the volume differences across all modes. Additionally, the correlation strength diminished between tumor amplitude and volume differences when the breath frequency was slowed to 5 bpm as shown in Figure 10. Pearson's correlation coefficients were 0.670, 0.675, and 0.691 for fine, normal, and coarse modes, with p<0.001 for all modes.

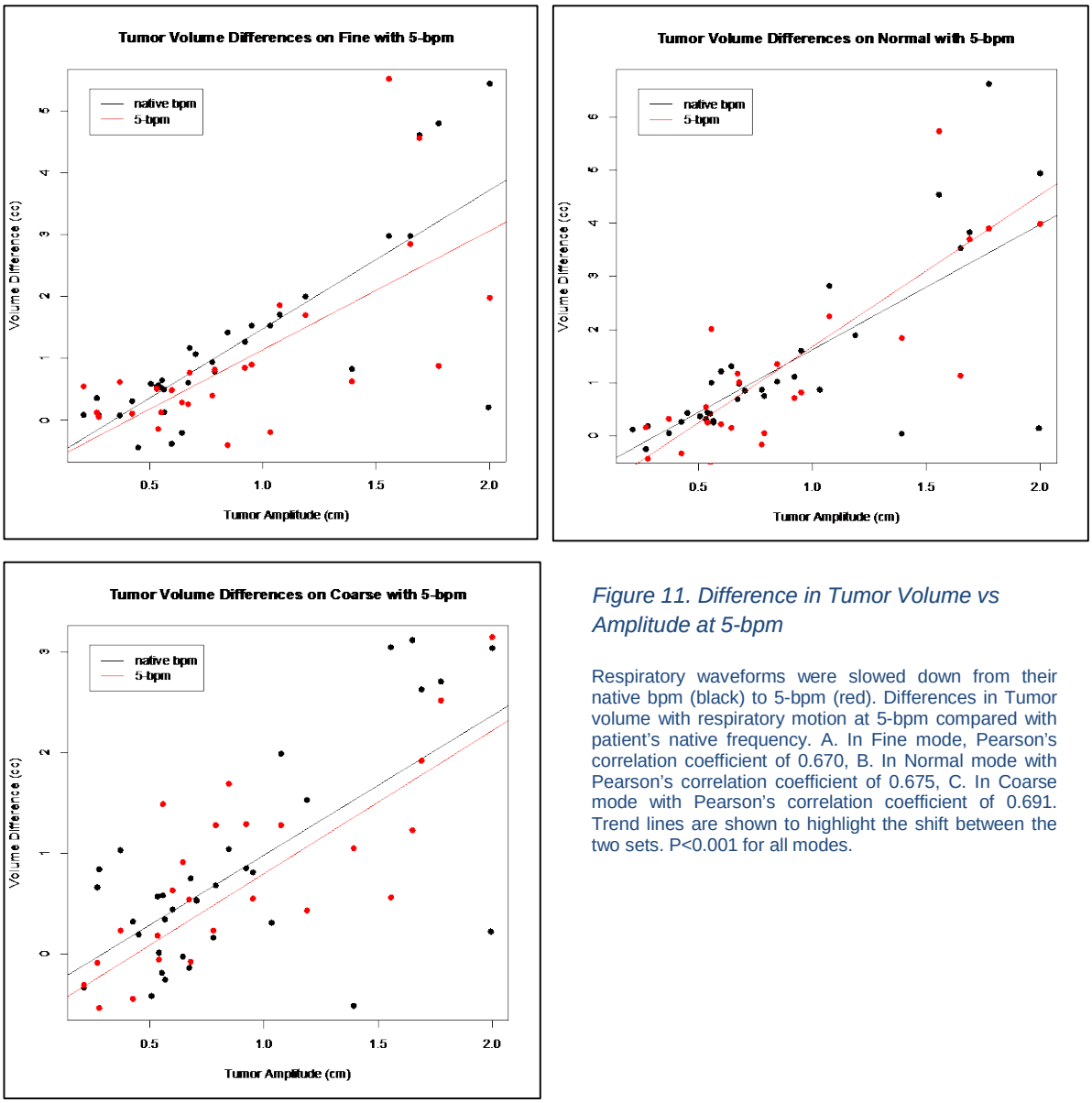

Figure 11. Difference in Tumor Volume vs Amplitude at 5-bpm

Respiratory waveforms were slowed down from their native bpm (black) to 5-bpm (red). Differences in Tumor volume with respiratory motion at 5-bpm compared with patient's native frequency. A. In Fine mode, Pearson's correlation coefficient of 0.670, B. In Normal mode with Pearson's correlation coefficient of 0.675, C. In Coarse mode with Pearson's correlation coefficient of 0.691. Trend lines are shown to highlight the shift between the two sets. P<0.001 for all modes.

5.4 Discussion

5.4.1 Impact of Breath Frequencies on MVCT

The hypothesis that increased breath frequencies would lead to larger imaging errors was not supported by the data in this study, although this may be a sample size issue. Only 3 respiratory waveforms had average breath frequencies of 10 bpm or less. No correlations between breath frequency and positional shifts nor volume measurements were observed across the cohort. For a given waveform, however, when the breath frequency was slowed to 5 bpm, there was a statistically significant, though clinically irrelevant, average inferior shift of 0.06 cm.

5.4.2 Impact of Tumor Amplitude on MVCT

The data in this study supports the hypothesis that larger tumor amplitudes result in larger imaging errors, specifically in volume differences. A moderate to strong correlation between tumor amplitude and volume differences was observed, with the strongest correlation for the fine MVCT mode.

5.4.3 Clinical Impact

Despite some statistically significant findings, on average, the clinical significance is minimal. No indication of an interplay effect was notable in this study. This is likely attributed to how the MVCT scan volume exceeds the length of the ITV to ensure the moving tumor is captured on the images. Any interplay at the edge of the volume will not be evident. Additionally, the MVCT acquisition is performed with all binary MLCs in the open position; thus there will be no interplay between the leaf synchronization and the tumor motion. The only source of interplay is the tumor moving in and out of the scanning plane during image acquisition, and this is essentially manifested as a motion artifact. For radiation therapy, these motion artifacts are acceptable so long as the clinician can still interpret the position of the tumor and critical structures, and position the patient correctly.

Regarding the different MVCT modes, all imaging modes resulted in overestimation of the tumor volume, which is attributed to the presence of motion artifacts on the images. A tumor with large blurring effect would result in a larger volume when contoured. The variance between all 3 modes were similar, though slightly smaller for coarse, which is likely due to the higher scan speed. The tumors in the coarse images were overall blurrier, but were not discontinuous like some of the images acquired in fine mode. The risk of a higher scan speed, however, is the possibility of missing part of the tumor, particularly if the tumor is small. The $tumor_{plastic}$ has a diameter of 3-cm, which is relatively large. An insert with a smaller plastic tumor would be required to test the resolution limits of the coarse mode. Use of the fine MVCT mode resulted in fewer and smaller z-positional errors than normal and coarse, at the expense of potentially larger and uglier motion artifacts.

In the context of the ASTRO guidelines that recommend an error tolerance of 0.1 cm for SBRT imaging systems, several cases exceeded this limit: 9 cases with fine mode, 11 cases in normal mode, and 12 cases in coarse mode. The largest absolute Z-shifts recorded in fine, normal, and coarse modes

were 0.16 cm, 0.31 cm, and 0.57 cm, respectively. The clinical impact of shifts this large could be significant, depending on the clinical situation.

Given the existence of variation and error in positioning, especially considering that patients move and breathe irregularly, an additional margin is commonly added to account for these setup variations. Giglioli *et al.* performed a multi-institutional planning comparison where a 0.3 cm expansion of the ITV was applied (55), and the RTOG 0236 trial specified a maximum margin of 0.5 cm in the axial dimension and 1.0 cm in the superior-inferior dimension (18). Certainly, a margin of 1.0 cm would cover the largest shifts observed in this study, however, this increases the total volume irradiated and may be clinically unfeasible if the tumor is close to, or abutting, a critical area.

One contributing factor that was not originally considered in this study is the effect of abdominal compression. Normal and coarse were the only modes with Z-shifts larger than 0.2 cm. In normal mode, 5 out the 6 cases with shifts greater than 0.2 cm had no compression applied when the respiratory waveforms were recorded. In coarse mode, 5 out of 8 cases with shifts greater than 0.2 cm had no compression applied. It should be noted that for these cases, the tumor amplitudes varied widely from 0.44 cm up to 2 cm. The two cases with the largest shifts, Case 1 with -0.45 cm and Case 18 with -0.57 cm shifts, were both done without compression, and did not have the largest tumor amplitudes.

One explanation is free breathing more easily allows irregular respiratory patterns. Abdominal compression may encourage more regular and perhaps deliberate and shallower breathing, and it could be the regularity of the respiratory pattern that is primarily responsible for the cases with large z-positional errors.

The overall comparison between the MVCT images of a moving target for a variety of respiratory waveforms and tumor amplitudes indicates that using fine mode generates smaller errors in the Z-position. This is to be expected given the smaller scan resolution. However, the clinician should also be aware that discontinuous motion artifacts will also be evident in these images, as compared to normal and coarse.

5.5 Chapter Summary

Higher breath frequencies did not appear to have an impact on the ability of the MVCT to resolve a moving target, contrary to the original hypothesis. Cases with higher tumor amplitudes did present with an average inferior shift of 0.154 cm compared to stationary baseline, while the low amplitude cases were only 0.05 cm inferior. These shifts, however, are likely not clinically relevant given the general practice of adding planning margin on the order of 0.3 to 1.0 cm. Additionally, abdominal compression may play a role improving MVCT accuracy for moving targets. The preliminary data in this study suggests that abdominal compression may improve regularity of the respiratory pattern, while also reducing the tumor amplitudes, which in combination may improve the accuracy of TomoTherapy MVCT scans for SBRT pre-treatment verification.

Chapter 6. Interplay Effect: TomoTherapy SBRT Dose

6.1 Introduction

As described in Chapter 3, a common method for SBRT treatments is referred to as an ITV-approach. Briefly, the ITV is the CTV with some margin added to account for internal physiologic movement and variations in size, shape, and position. It is commonly defined using a 4DCT scan that employs a slow CT acquisition protocol coupled with a respiratory signal to create a model of the patient's anatomy during a single breath cycle. In a perfect system, the ITV-based approach should account for all possible tumor positions while the patient is breathing. Realistically, however, this method is based on a number of assumptions. One assumption is that the tumor displacement measured on the 4DCT images represents the boundaries of all possible tumor locations regardless of changes in breath frequency or other respiratory waveform characteristics. A second assumption is that as long as the patient is positioned correctly and the tumor does not move outside the boundaries of the ITV, the radiation therapy system will deliver the planned dose to the tumor, even if the respiratory waveform has changed. Essentially, the assertion of the ITV method is that how the tumor moves does not affect the dose it will receive. The existence of the interplay effect for TomoTherapy challenges this assertion because the coincidence of the superior-inferior tumor motion with the longitudinal direction of the couch motion may lead to dose discrepancies between the delivered and planned dose distributions. For conventional radiation therapy where 20-30 treatments are given, these dose discrepancies arguably average out (13,48,49).

The hypothesis of this study is that higher breath frequencies and larger amplitudes will correspond with larger dosimetric errors, specifically a reduction in tumor dose. The objective is to quantify the dose discrepancies for SBRT treatments, and determine how the interplay effect is influenced by the patient's breath frequency or amplitude of tumor displacement.

6.2 Methods

As described in Chapter 4, a cohort of 35 respiratory patterns was used to program the Quasar motion phantom to simulate each patient's lung tumor trajectory during respiration. To allow further investigation into the effect of a slower breath frequency during treatment, the respiratory patterns were also stretched to simulate a breath frequency of 5 bpm. Throughout the rest of this manuscript, references to the patient's actual breath frequency will be referred to as "native breath frequency."

6.2.1 4DCT Simulation of Motion Phantom

Each of the 35 respiratory patterns were uploaded and programmed into the Quasar motion phantom, and an SBRT simulation was performed. The SBRT simulation included a CT scan (3D-CT) of the phantom with the plastic tumor stationary to serve as the primary planning scan, and a 10-phase 4DCT scan with the plastic tumor in motion at the native breath frequency. These two imaging studies

were transferred to the MIM contouring workstation where the plastic tumor was outlined using auto-contouring tools and a preset window-level setting. The plastic tumor was contoured on each of the 10-phase datasets of the 4DCT and summed to form the ITV (Figure 12). No additional margin was added to the ITV. A 5-mm ring was drawn around the ITV to serve as a constraining structure to avoid dose spillage outside of the ITV.

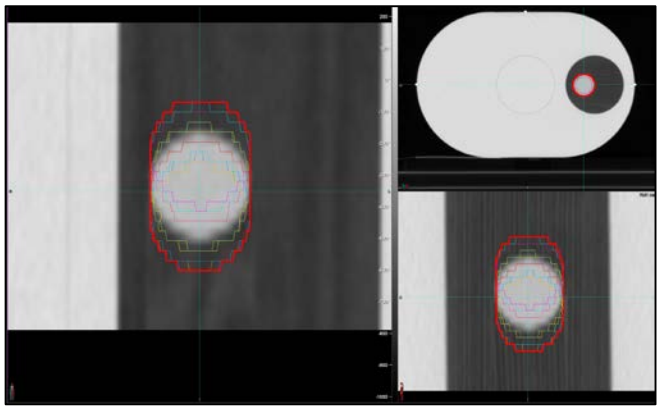

Figure 12. ITV on Case 6. The bold red outline represents the ITV (internal target volume) which is the Boolean sum of the tumor contoured on each phase during 4DCT. The thin colored lines are the outlines of the tumor on the different phases of a 4DCT.

6.2.2 TomoTherapy SBRT Plan

To investigate the dosimetric effects of the interplay effect, the goal was to design treatment plans that were clinically feasible, requiring a reasonable fraction dose that was also deliverable within an acceptable time frame. Given the large number of ways to generate such a plan with two different jaw widths, different pitches, and modulation factors, I focused on creating SBRT plans that I thought were most likely to expose an interplay effect. Bounded by the gantry period limits of the system, minimum of 12 seconds/rotation (s/rot) and maximum of 60 s/rot, I chose to build plans with the fastest gantry rotation (12 s/rot). A slow gantry rotation would allow a moving tumor to pass in and out of the radiation field multiple times, thus causing any interplay effects to average out.

Next, the dose needed to be large enough to be clinically plausible for an SBRT treatment. At the Queen's Medical Center, common SBRT fraction doses are between 12 Gy and 20 Gy per fraction. Due to mechanical limits of the machine, these SBRT treatments often require multiple "passes" of smaller doses that are delivered sequentially to the patient in one treatment session. For example, an SBRT fraction of 15 Gy would be given using 2 passes of 7.5 Gy in one appointment. Based on preliminary plans, a dose around 7.2 Gy (range 7.0 to 7.6 Gy) to 95% of the ITV was found to be deliverable with a gantry period of 12 seconds/rotation. This required the use of the 2.5-cm jaws, modulation factor around 1.2 and a pitch of 0.1. The plans were designed to give a homogenous dose to the ITV to exclude the possibility that any observed dose variations might be attributed to a hotspot inside the ITV rather than

the interplay effect. An example of an SBRT plan is shown Figure 13. The treatment times for these plans average 5.5 minutes (range 4.7 to 6.24 minutes). No additional margins were added to the ITV.

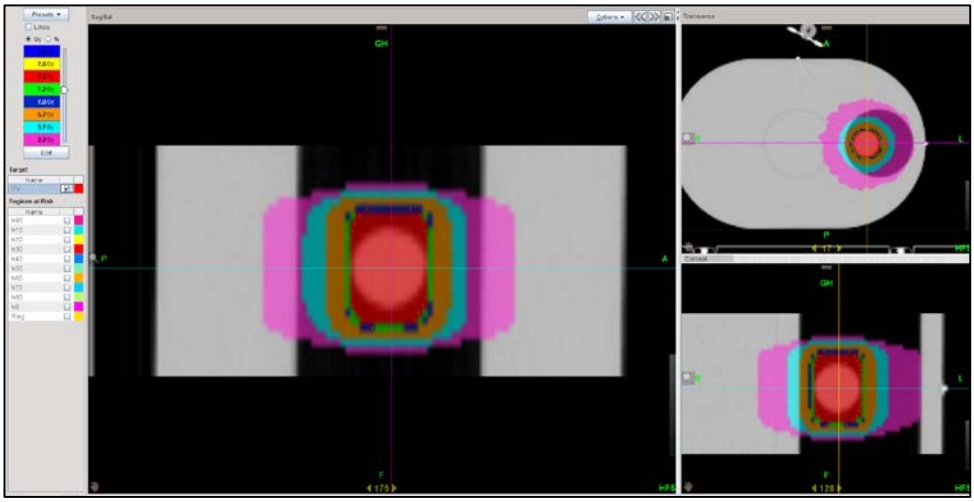

Figure 13. SBRT Plan for Case 6. Red shaded region corresponds to the prescription dose of 7.4 Gy.

Each plan was delivered to the motion phantom a total of 10 times to obtain ion chamber and film measurements, with the phantom stationary, in motion at the native breath frequency, and with a breath frequency of 5 bpm.

6.2.3 Ion chamber and Film measurements

Two different inserts were used with the Quasar motion phantom: one insert contained a plastic tumor with a hole drilled to fit an Exradin A1SL ion chamber, and another insert with a plastic tumor but split down the center to allow placement of a piece of film. The A1SL chamber was connected to a Standard Imaging TomoElectrometer unit to collect the charge, with appropriate temperature and pressure correction applied. The TomoElectrometer was connected to the TomoTherapy Electrometer Measurement System (TEMS) to record the collected charge every 200 msec. This provided real-time visualization of the interplay between the moving tumor and the helical delivery of dose. The baseline measurements were collected with the plastic tumor stationary. Two additional sets of ion chamber measurements were made: one with the plastic tumor moving with the patient's native respiratory breath frequency, and the other with the respiratory waveform stretched out to average a breath frequency of 5 bpm. Each of these conditions was measured 3 times to characterize the effective variance due to the moving plastic tumor, and also to simulate a 3-pass SBRT treatment.

The film used was GafChromic EBT3 film (Radiation Products Design Inc., Albertville, MN), all from the same batch (Lot#12291501). Each sheet of film was carefully cut into 6 pieces, with care to maintain the same orientation with each other. A dose calibration film was irradiated from 10 cGy up to 9 Gy to convert pixel values to dose. Each film was scanned using a Vidar Dosimetry Pro Advantage Red

scanner 48 hours post-irradiation. One film exposure was made with the plastic tumor stationary, one exposure with the tumor moving at the patient's native breath frequency, and one exposure with the respiratory frequency stretched to 5 bpm. The stationary film was used as the baseline against which the subsequent motion films were compared. Co-registration of the film using fiducials was performed using ImageJ software (NIH, v1.51j), and all film analysis including gamma, flatness, and penumbra calculations were performed using DoseLab Pro v6.60 (Mobius Medical Systems, Houston, TX).

Gamma is the percent of pixels in a 2D image that pass given criteria. The criteria used were <2% dose difference or <2 mm distance-to-agreement. Flatness and penumbra are measurements performed on a profile along the central axis of a 2D image. The flatness definition used here is described in Equation 4:

(4) $$Flatness\ (F) = \pm 100\%\ \frac{(\max value - \min value)}{(\max value + \min value)}$$

If the minimum value is closer to the center than the maximum value then the flatness is recorded as positive. The penumbra is defined as the distance between the 20% and 80% values on the profile, and describes the width of the field edge gradient (Figure 14).

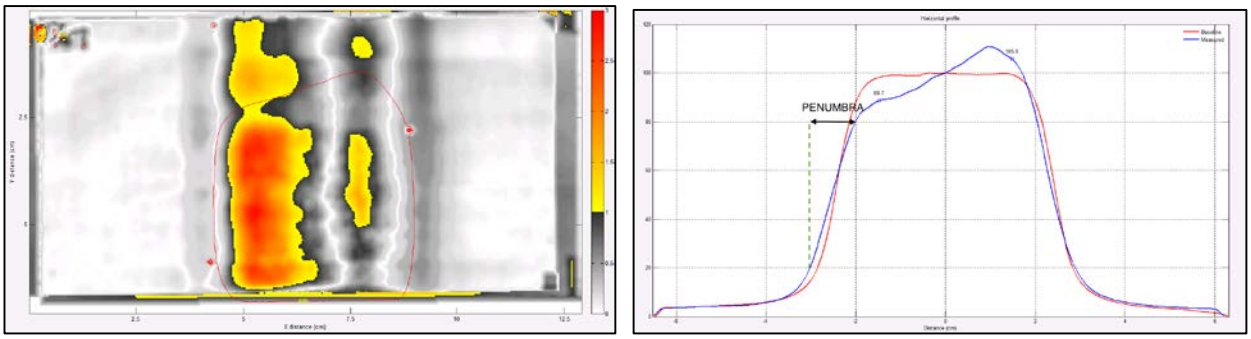

Figure 14. Gamma Analysis (left) and Penumbra (right) Analysis (Case 42). The yellow and red areas of the left image indicate regions on the film that are hotter than the tolerance of 2%/2-mm distance-to-agreement. The black arrow on the right profile illustrates the definition of penumbra: horizontal distance between the 20% and 80% regions on the profile.

6.3 Results

6.3.1 Overall Dose Differences

The dose differences between the stationary and moving $tumor_{plastic}$ were compared. A paired-samples t-test was conducted to compare the dose measured with the phantom at rest and in motion at the native breath frequency. There was no significant difference between the doses for the stationary and motion conditions (*p=0.961*). There were, however, 4 cases where the individual measured doses with the $tumor_{plastic}$ in motion were greater than 2% different from the stationary dose. Case 42 had the largest average dose difference of -0.32 Gy (-4.4%). During one reading, a dose difference of -0.56 Gy (-7.8%)

was measured. The average dose difference for Case 6 was -0.18 Gy (-2.4%), with one of the measurements giving a dose difference of -0.367 Gy (-5%.)

6.3.2 Impact of Tumor Amplitude

To explore how tumor amplitude influences the dose to the $tumor_{plastic}$, the dose differences were stratified by tumor amplitude (low <0.6 cm with n=14, high ≥0.6 cm with n=21), and an independent-samples t-test was conducted. There was no significant difference in the dose difference between motion and stationary between the two groups.

Next, I evaluated how tumor amplitude might influence the standard deviation of the dose measurements (Figure 15), using the same stratification, by conducting an independent-samples t-test. Higher amplitude motion resulted in larger standard deviation (mean=5.0 cGy) in the measured dose compared with lower amplitude motion (mean=2.1 cGy) with *p=0.025*. A Wilcoxon rank sum test was also conducted and the result was a significant difference (*W=219*, *p=0.015*).

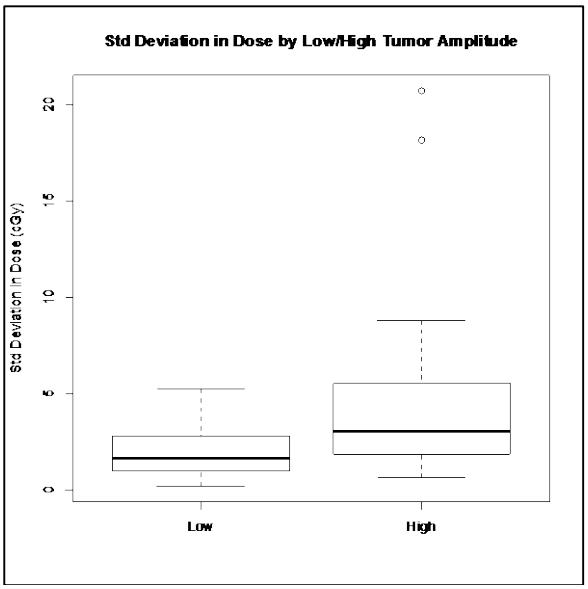

Figure 15. Std Deviation in Dose by High vs Low Tumor Amplitude

6.3.3 Impact of Breath Frequency

I compared the dose differences between the stationary and motion conditions, of waveforms with a fast breath frequency (fast ≥20 bpm, n=9) against the rest of the cohort (n=26). An independent-samples t-test was conducted and found the fast-bpm group had a smaller mean absolute dose difference (*M=0.*02 Gy) compared to the slower-bpm group (*M=0.06)* with a *p-value of 0.006* (Figure 16).

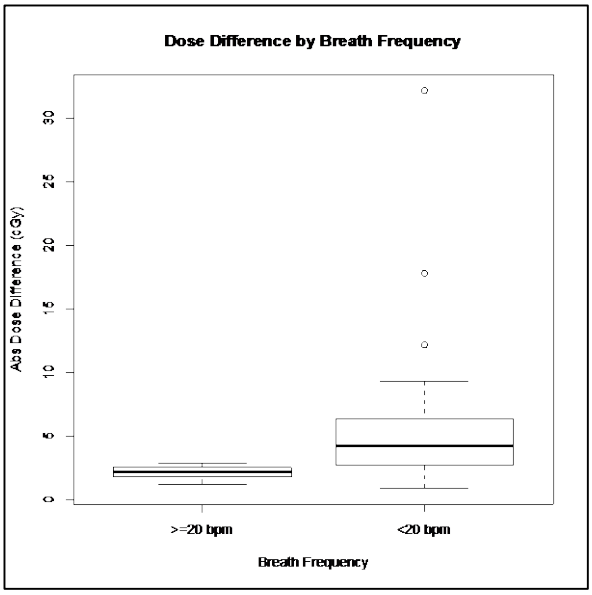

Figure 16. Absolute Dose Difference by Breath Frequency

To determine how higher breath frequencies might influence the variance of the measurements, using the same stratification, an independent-samples t-test was conducted. There was a significant difference found in the standard deviation of fast breath frequency measurements (mean=2.0) compared with slower breath frequency measurements (mean=4.5), with p = 0.025 (Figure 17).

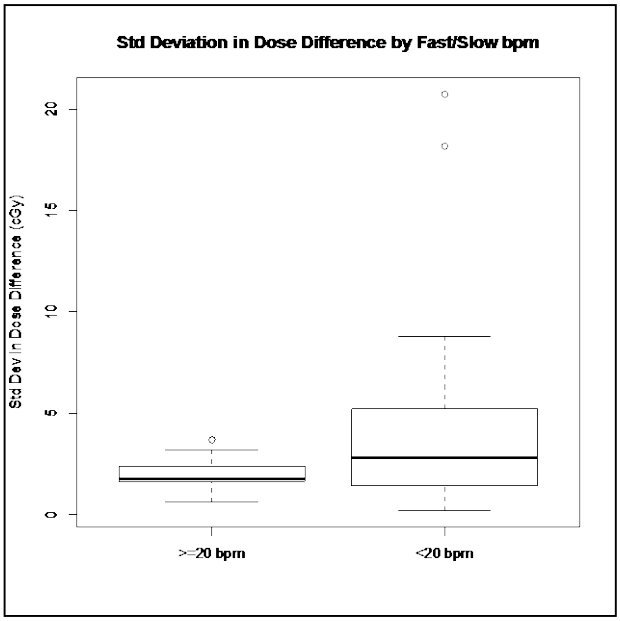

Figure 17. Std Deviation in Dose by Breath Frequency

6.3.4 Impact of Reducing the Breath Frequency for a Given Waveform

To further investigate the consequences of a reduced breath frequency compared to the native respiratory frequencies, the expanded (5-bpm) waveforms were also evaluated. Dose measurements with the $tumor_{plastic}$ moving at 5-bpm were compared against the stationary (baseline) measurements to isolate the effect of motion at a slower breath frequency. Figure 17 is an example of the time-based charge collection during the treatment with the $tumor_{plastic}$ stationary (left), moving at 5-bpm (middle), and moving at the native-bpm (right). The peaks in the stationary chart are due to the gantry rotation of the radiation beam; as the radiation nears the tumor, there is a spike in charge, and as the radiation rotates away from the tumor, the charge drops. Note that the charge does not drop to 0 nC, indicating that the $tumor_{plastic}$ is continuously being irradiated in the static scenario. In the 5-bpm chart, the same peaks as the stationary chart are evident, however, the dips are much lower and the peaks are spread out. This difference in charge collection is due to the interplay between the moving $tumor_{plastic}$ and the rotating gantry. Finally, in the native-bpm chart, the $tumor_{plastic}$ is moving into and out of the beam at a higher rate than 5-bpm, so there is a blurring of the overall distribution.

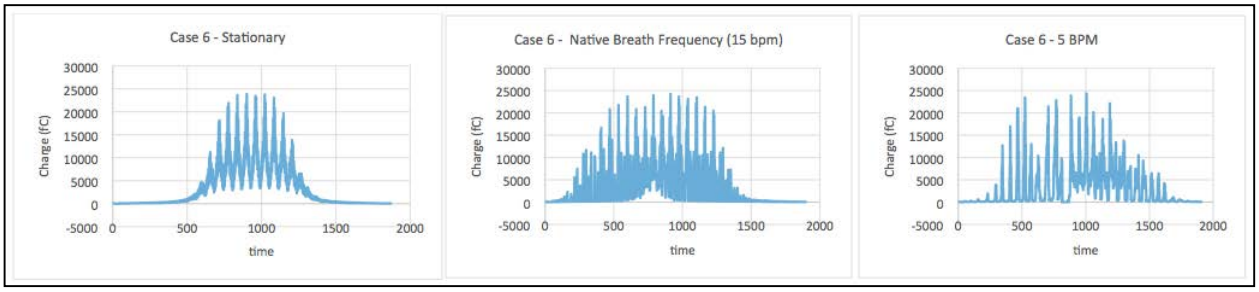

Figure 18. Ion Chamber Readings using TomoElectrometer Measurement System (TEMS). Graphical representation of the charge collected every 200 ms with the phantom stationary, in motion at patient's native breath frequency (15 bpm for Case 6), in motion at 5-bpm

A comparison of the measured dose between the stationary, motion at native breath frequency, and motion at 5-bpm is shown below in Figure 19. The dotted red lines indicate the +/-2% tolerance from the average of the stationary dose measurements.

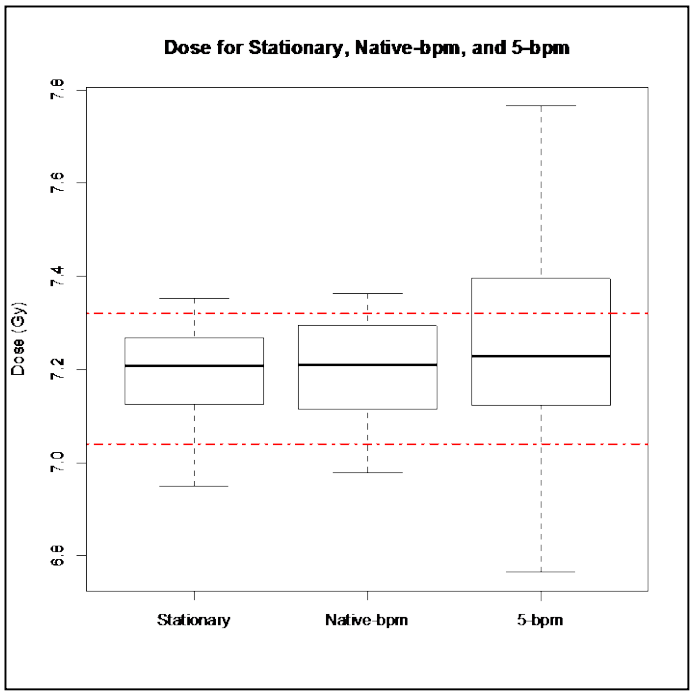

Figure 19. Comparison of Measured Dose for Stationary, Native-bpm, and 5-bpm

A paired-samples t-test found the 5-bpm measurements had an average reduction from static measurements of -0.08 Gy with p=0.00409. Only 8 respiratory waveforms at 5-bpm had doses within 2% from the stationary dose. The remaining 27 cases had at least one measurement that exceeded the 2% threshold, with Case 10 having the largest average dose difference of 0.454 Gy (-6%). The largest dose discrepancy measured was -1.38 Gy (-19%) for Case 39.

To determine if on average, the native bpm data were closer to the static measurements compared with the 5-bpm data, I conducted a paired-samples t-test. There was a significant difference in the average dose difference for the 5-bpm (M=7.75, SD=16.57) and native-bpm (M=-0.06, SD=7.44) conditions; p=0.026. Figure 20 illustrates the wider range of dose differences in the 5-bpm condition compared with the native-bpm.

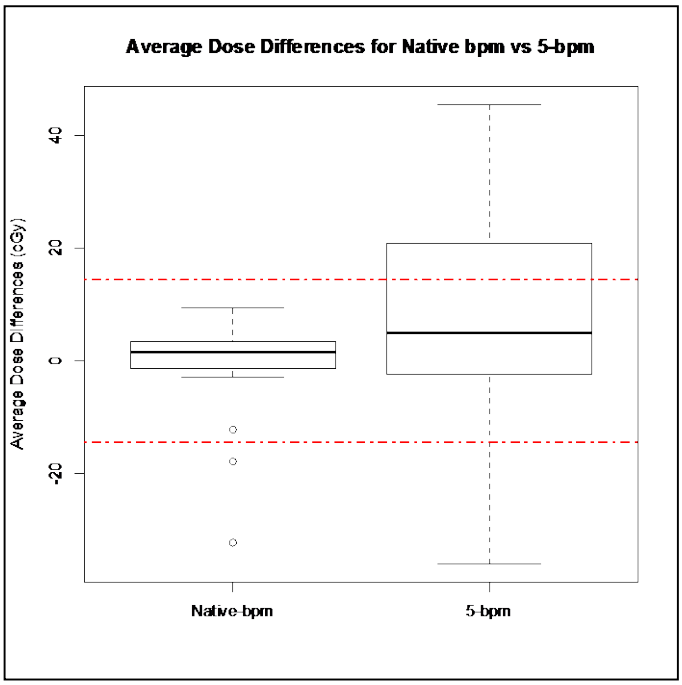

Figure 20. Average Dose Difference for Native-bpm and 5-bpm, relative to stationary dose as baseline. A negative difference means the dose was less than the stationary dose. Dotted red lines indicate ±2% of the average stationary dose

Next, I explored the standard deviation between each measurement at 5-bpm compared with the variance between each measurement at the native-bpm. The average standard deviation of dose in the 5-bpm measurements was 0.2 Gy larger (approximately 2.7% of the prescription) using a paired t-test, p = 3.016e-06. Figure 21 illustrates the standard deviation of the measurements at 5-bpm compared with the native-breath frequencies across the cohort. A wilcoxon rank sum test was also performed and determined a significant difference between the native-bpm and 5-bpm standard deviation (*p<0.001)*.

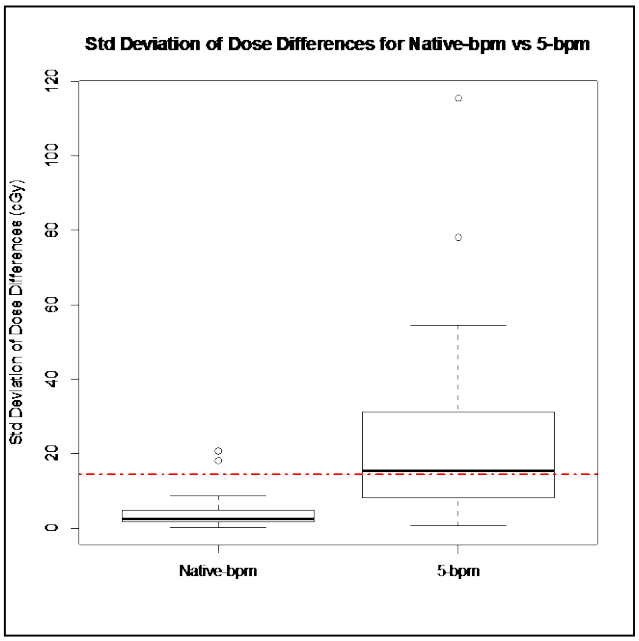

Figure 21. Std Deviation of Dose Differences for Native-bpm and 5-bpm across Cohort; Dotted red line indicates the 2% tolerance recommended by ASTRO

The disparity in standard deviation across the cohort is evident in each case. Figure 22 shows an example of the variability in dose when the respiratory waveform in Case 18 moves at 5 bpm compared with the native breath frequency of 20 bpm.

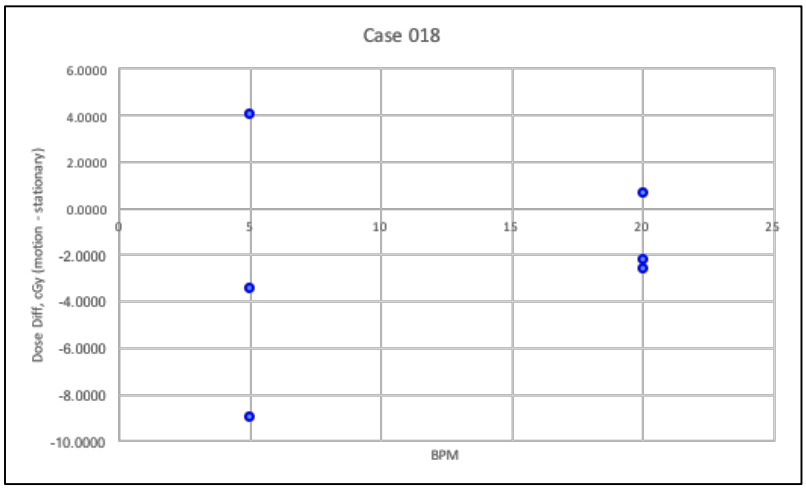

Figure 22. Std Deviation of Dose Differences for 5-bpm and Native-bpm for a Single Case. Illustrates an example of the difference in dose measured 3 times with the respiratory waveform at 5-bpm vs 20-bpm for Case 18.

Stratification of the 5-bpm data between low and high tumor amplitudes was done, and an independent-samples t-test was conducted. The high tumor amplitude standard deviation in dose (mean=33.29) was significantly larger than the low amplitude measurements (mean=10.63), with *p=0.001*.

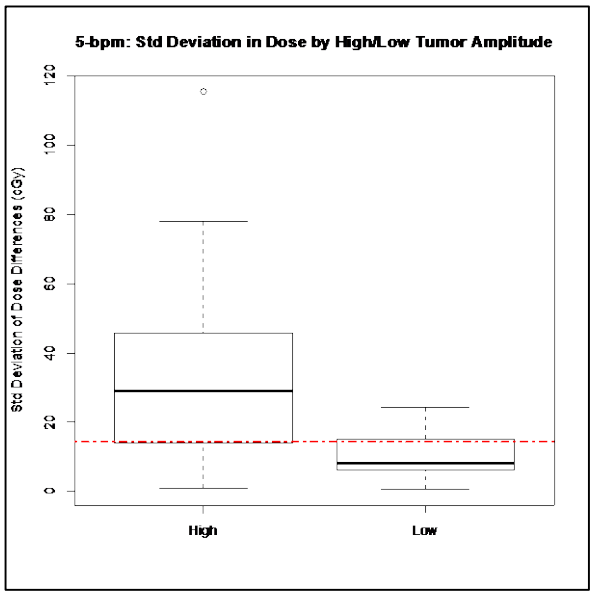

Figure 23. 5-bpm: Std Deviation in Dose by High/Low Tumor Amplitude; Dotted red line indicates 2% tolerance per ASTRO recommendations

At the reduced breath frequency of 5-bpm, larger tumor amplitudes appear to have a greater influence on the standard deviation of dose. A Pearson's correlation coefficient was computed to assess the relationship between tumor amplitude and the variance in dose measurements. There was a positive correlation between the two variables though moderate in strength (r=0.682). A scatter plot summarizes the results in Figure 24.

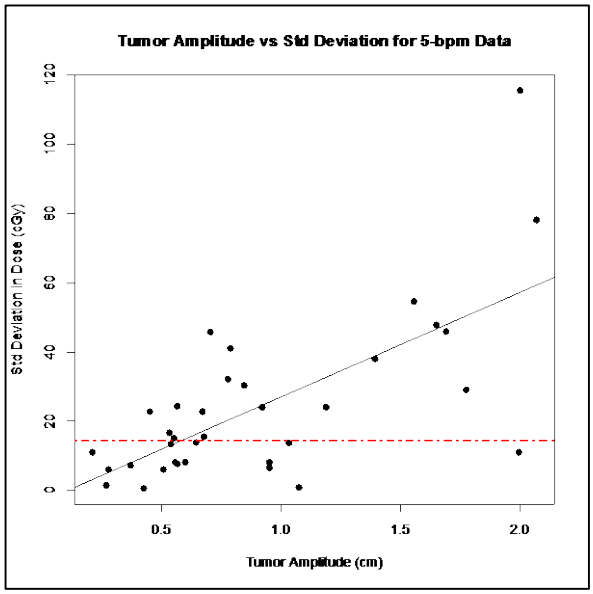

Figure 24. Std Deviation in Dose vs Tumor Amplitude for 5-bpm Data; Dotted red line indicates 2% tolerance per ASTRO recommendations

6.3.5 Film Comparison

No significant differences in the gamma was determined. The difference in flatness between low and high amplitude conditions was significant ($p = 0.03202$) with an average increase in flatness of 2.594 with high tumor amplitudes. The tumor amplitude was strongly correlated with flatness (r = -0.873; Figure 25).

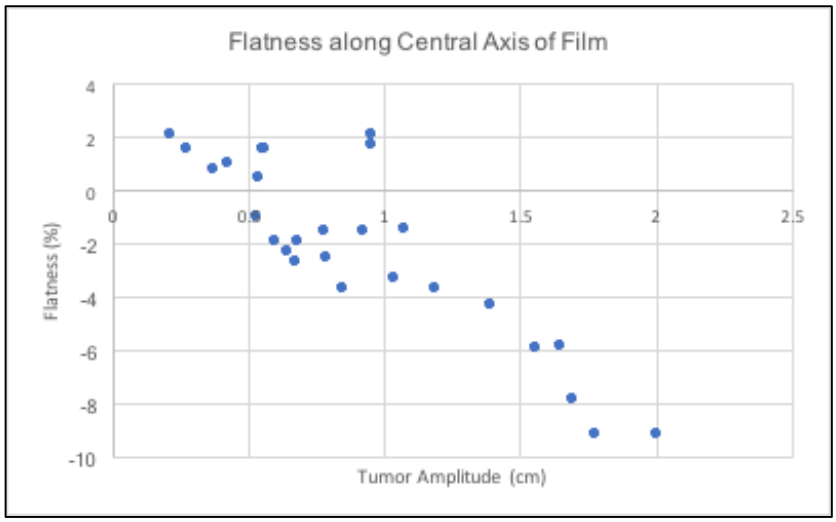

Figure 25 Correlation of Flatness with Tumor Amplitude. Flatness determined along the central axis of film for each waveform vs the corresponding tumor amplitude (cm). Pearson's correlation coefficient is -0.873.

There was also strong correlation between the tumor amplitude and the width of the penumbra (defined as the distance between 20% and 80% on the center profile), with correlation coefficients of 0.959 on the left-sided penumbra and 0.940 on the right-sided penumbra.

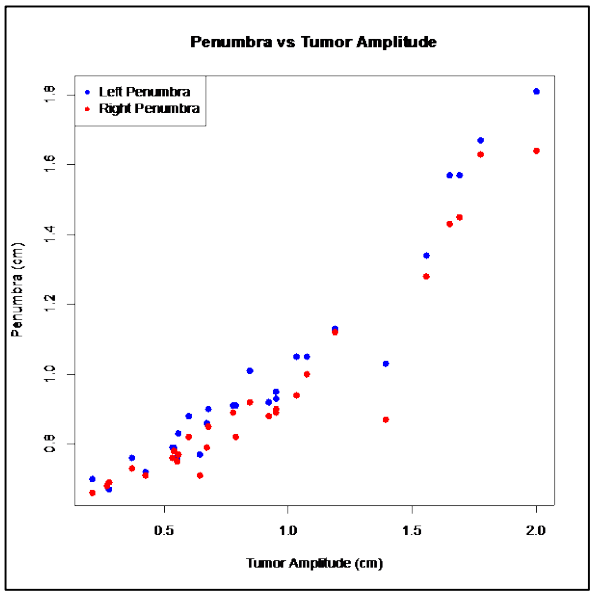

Figure 26 Correlation of Left and Right Penumbra with Tumor Amplitude. Penumbra, measured as the distance between the 20% and 80% values on profile along the central axis of each film) vs the corresponding tumor amplitude (cm). Pearson's correlation coefficient of 0.959 for left-sided penumbra and 0.940 for right-sided penumbra.

A paired-sample t-test of the absolute value difference in flatness for film exposed with the respiratory waveforms at 5-bpm and native breath frequencies was conducted. There was a significant difference (p=0.0001) with the film exposed at 5-bpm compared with native-bpm, with a mean of the differences of 3.84. Results are shown in Figure 27. An example of the flatness measurements of the film for case 42 are shown in Figure 28.

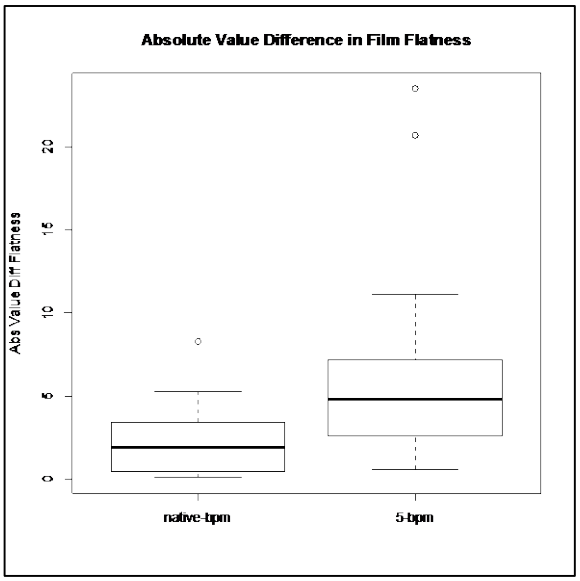

Figure 27. Absolute Value of Difference in Film Flatness between 5-bpm and Native-bpm

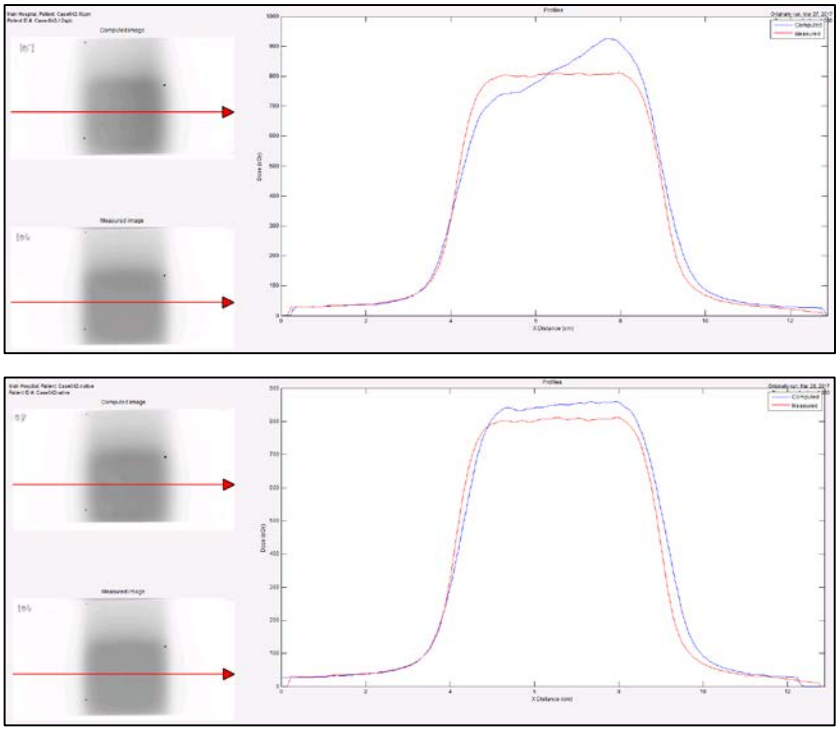

Figure 28. Film Flatness Comparison for Case 42. Red profile is the static film, Blue profile (Top) is the 5-bpm film, Blue profile (Bottom) is the native-bpm film.

6.4 Discussion

The hypothesis that higher breath frequencies would lead to larger dosimetric errors due to the interplay effect is not supported by the data presented here, where the opposite seems to be the case. Patients with faster breath frequencies had smaller absolute value dose differences and smaller variances than those with slower breath frequencies (<20 bpm). Furthermore, when the respiratory waveforms were simulated to have a breath frequency of 5-bpm, the variation in measured dose increased. Film analysis did not expose any noticeable breath frequency-related effects, other than a significant difference in film flatness between the native-bpm and 5-bpm film.

However, the findings do support the hypothesis that higher tumor amplitude will result in increased dose differences. Within the native-bpm data, standard deviation of dose increased slightly for the larger tumor amplitude cases. The correlation between tumor amplitude and variance, however, was much stronger in the 5-bpm data. This suggests that slower respiratory waveforms together with larger tumor amplitudes (>0.6 cm) are more susceptible to larger variances in dose.

Despite the statistical significance of the results discussed above, the means of the differences were all relatively small and clinically insignificant when considered in aggregate. Upon closer examination, however, some results are concerning. For example, while the mean of the differences for the standard deviation of dose for the waveforms moving at their native-bpm was 0.2 Gy, there were 4

cases where the measured doses exceeded +/-2% of the baseline doses. In the 5-bpm data, 26 cases (74%) exceeded +/-2% of baseline. Some of these differences were as hot as +138.1 cGy (+18% of prescription), and as cold as -90.8 cGy (-12% of prescription). These findings suggest that a relaxed (slower) breath frequency will increase the dose discrepancy to the target volume compared to cases that maintain higher breath frequencies. The variability of the dose to the tumor will increase, likely beyond the 2% recommended tolerance.

Not surprisingly, larger tumor amplitudes did correlate with larger penumbra and larger variation in flatness across the central profile. Changes in penumbra ranged from 0 to 1.37 cm on the left and 1.17 cm on the right. This is the blurring effect on the edge of the film due to the tumor moving in the superior-inferior direction. A greater concern, however, is the effect on the flatness of the radiation field. The SBRT plans in this study were designed to deliver a homogeneous dose distribution across the entire length of the ITV. With larger tumor amplitudes, however, we see this homogeneity disturbed such that there are bands of higher dose followed by bands of lower dose. This is represented two-dimensionally in the profiles and also visible on film analysis. Figure 29 provides examples of the film analysis for Case 6. The image in the top-left shows the relative percent difference between the native-bpm film and the static film after they have been coregistered. Note the bands of red (static film is hotter than native-bpm film) and blue (static film is cooler than native-bpm film). The image in the top-right shows areas of the film that exceed the gamma tolerance of 2%/2mm. The bottom image shows the profiles between the static film (red) and the native-bpm film (blue).

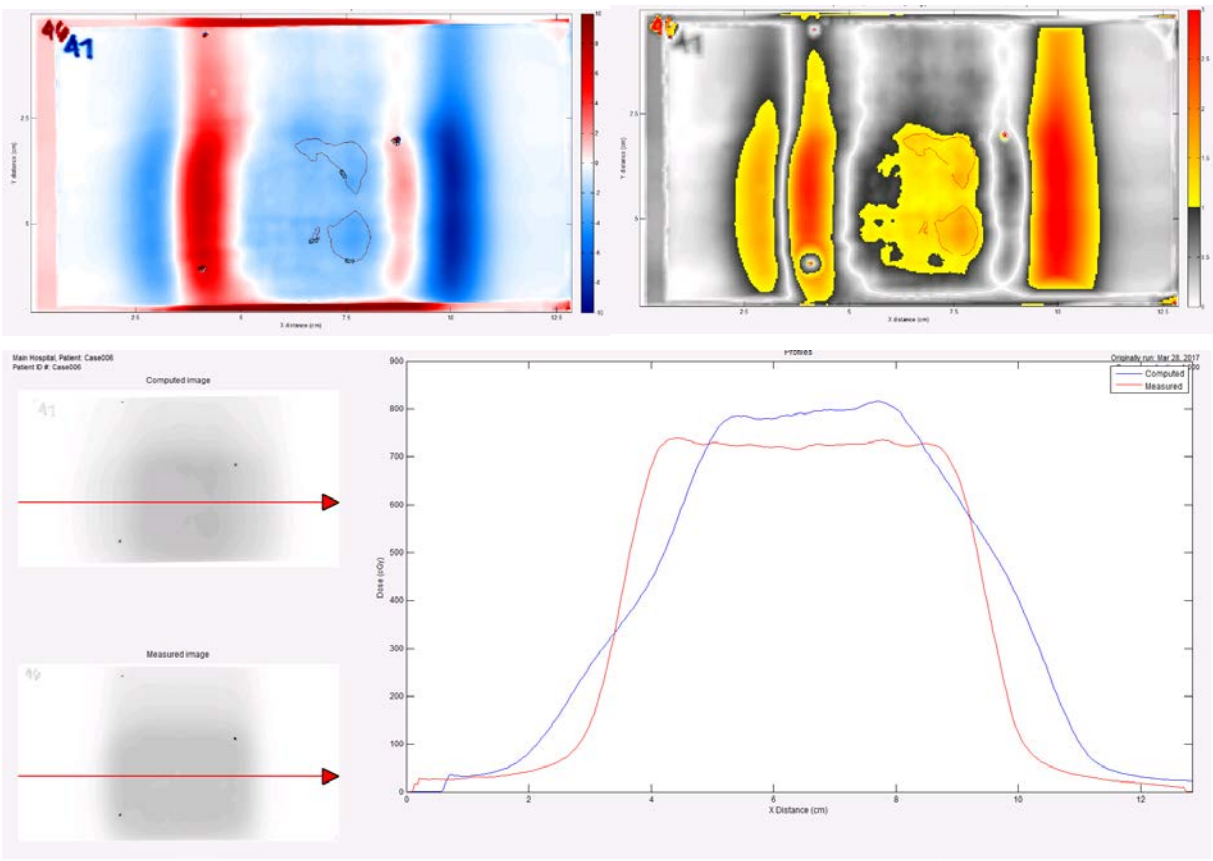

Figure 29. Film Analysis for Case 6. Red profile is stationary film and Blue is 5-bpm.

This effect is amplified when the breath frequency is slowed to 5 bpm. With large tumor amplitudes and slow breath frequency, such as shown below in Figure 30 for Case 39, the effect is quite pronounced. This suggests that while breath frequencies did not indicate a large clinical difference with ion chamber measurements, on film, the interplay effect seems to be more evident.

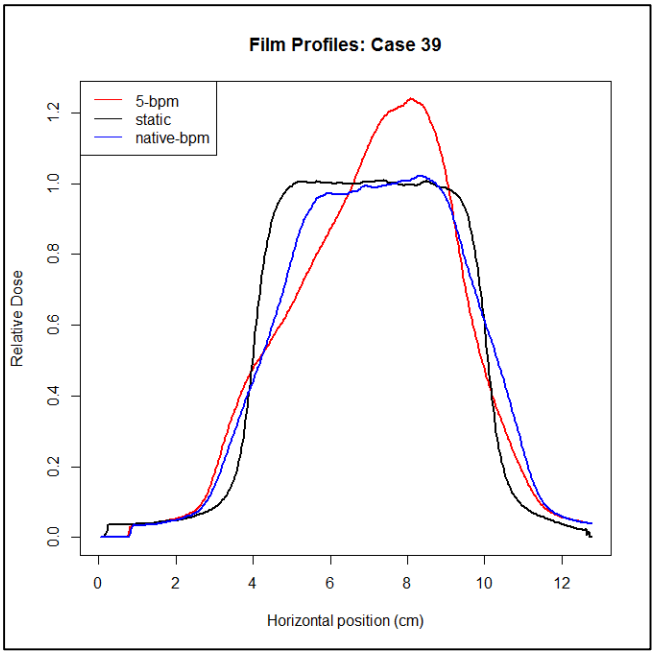

Figure 30. Film Profiles for Case 39

As an exercise to estimate the impact of the observed variance in the context of a 3-pass SBRT treatment, the 3 measurements made with the waveform at 5-bpm and at the native bpm were summed and compared with 3 times the stationary dose. The largest difference in dose between the native-bpm and stationary condition was -0.96 Gy (-4.5% of the stationary dose) to +0.28 Gy (+1.3%) with an average across the cohort of -0.002 Gy (-0.5%). For waveforms slowed to 5-bpm, the difference in dose ranged from -1.08 Gy (-5%) to +1.36 Gy (6.2% of the stationary dose) with an overall average of +0.23 Gy (+1.1%). This suggests that for the majority of patients, the interplay effect will likely not be a clinical concern. However, there are a few cases where it might require consideration. A closer look at particular cases highlights a few nuanced details.

6.4.1 Cases 6 and 40:

Case 6 showed the largest measured dose discrepancy of -0.557 Gy (-7.4% of the prescription) with an average dose discrepancy of -0.322 Gy (-4.3%). This case also had the largest standard deviation of 0.207 Gy (2.8% of the prescription). The respiratory pattern for this case came from a patient who had a tumor in the posterior right lower lobe. The 4DCT was acquired without abdominal compression, and showed a tumor moving with an amplitude of 2.07 cm and a breath frequency of 15 bpm. Because of the large tumor amplitude, a second 4DCT was performed with abdominal compression in an attempt to reduce the amount of motion. The tumor amplitude decreased slightly to 1.7 cm and the breath frequency increased to 20 bpm. This second set of 4DCT images and associated respiratory pattern is represented

in Case 40, where the maximum dose discrepancy reduced to -0.035 Gy (-0.5% of the prescription) with a variance of 0.024 Gy (0.3% of the prescription).

In this situation, because the tumor displacement was still relatively large even after abdominal compression was applied, this reduction in dose discrepancy and variance is likely due to another consequence of abdominal compression. One possibility is that abdominal compression caused increased breath frequency, which reduced the impact of the interplay effect. Alternatively, abdominal compression may cause patients to breathe with more regularity when compared to free breathing without compression, which may lead to reduced dose discrepancies between the stationary and motion conditions. Figure 31 illustrates a snapshot comparison between this patient's respiratory waveform without compression (blue) and with compression (green). The patterns appear similar, except for a few notable points. At around 26 seconds, this patient took a relatively short inhale indicated by the small blue bump. Without compression, the patient is free to breathe as quickly or deeply as they feel comfortable, and this irregularity may be a factor for the variance that we see between each treatment.

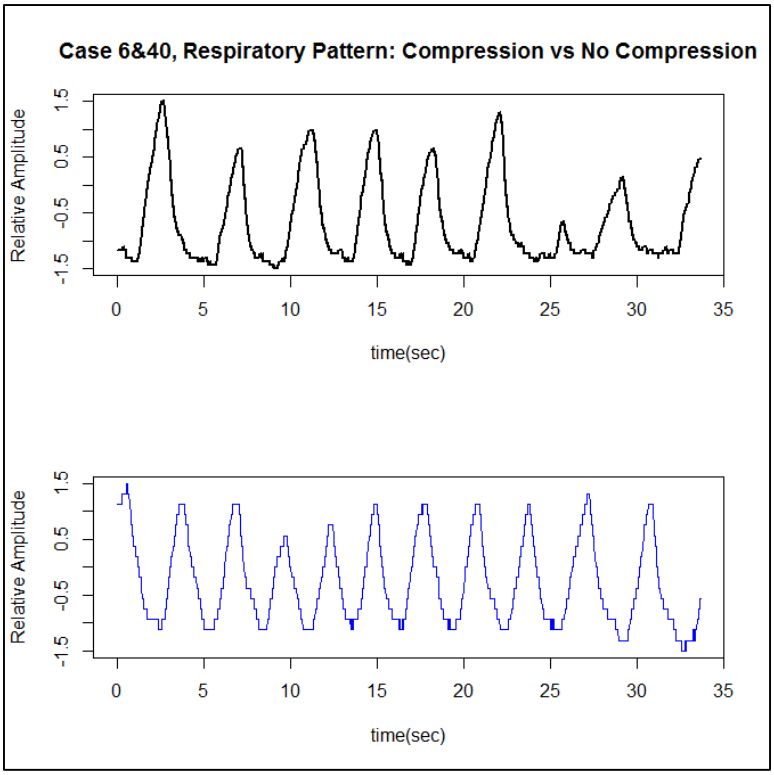

Figure 31. Comparison of Respiratory Waveforms for Case 6 and 40. For the same patient, case 6 represents the respiratory waveform without compression and case 40 is the respiratory waveform with compression.

6.4.2 Case 19 and 34

The second case to consider (case 19) is from a patient with a tumor in the left lower lobe that moved with amplitude of 0.95 cm and a breath frequency of 9 bpm without compression. This case demonstrated the largest positive average dose difference of 0.093 Gy (+1.2% of prescription). The

variance of the differences was 0.018 Gy, indicating that all 3 measurements were similarly different from the stationary measurements (0.102 Gy, 0.104 Gy, and 0.073 Gy.)

When compression was applied, the amplitude increased slightly to 1.03 cm, and the breath frequency also increased to 13 bpm. The respiratory data for the compression condition was classified as case 34 and resulted in an average dose difference of 0.011 Gy (+0.1% of prescription). Comparison of the respiratory patterns suggests in this case that the compression smoothes the exhale and appears to improve regularity of the pattern (Figure 32).

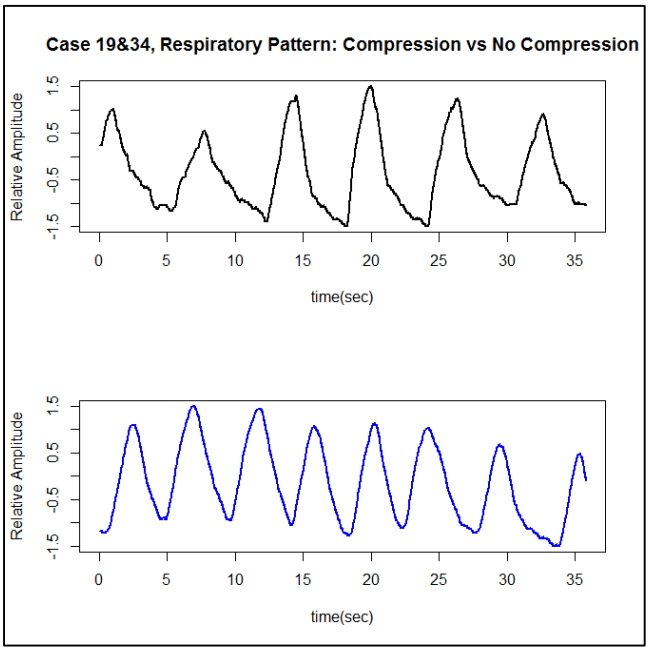

Figure 32. Respiratory patterns for with and without compression for a single patient (Case 19 and 34)

6.4.3 Limitations

There are several limitations to this component of the study. One limitation is that the variance is calculated from a sample size of 3 measurements. Despite this, however, the variance of the 5-bpm condition was widely different from that of the native-bpm. Another limitation is that the timing of the respiratory pattern and the actual onset of the TomoTherapy beam are not synchronized. During the data acquisition, attempts were made to vary the timing of the measurements so that no two measurements were made at the same phase, but this was not a precise method. Given that the respiratory patterns have irregular components, the timing of when the irregularity occurs during the treatment could have a significant impact for that particular measurement. A third limitation is that the impact of applying compression is unclear. In some cases, compression appears to improve reproducibility of results possibly by causing the patient to breathe more regularly. This effect, however, was not seen in all cases and more data is required to characterize the impact of compression.

6.5 Chapter Summary

Among this cohort of respiratory waveforms, ion chamber and film measurements provide some evidence of the interplay effect. Based on this study, slower breath frequencies are likely to result in larger dose differences compared with the stationary condition, and larger tumor amplitudes do result in larger dose differences, particularly at the penumbra. While the ion chamber results showed a clinically small difference, review of the film results suggests the interplay effect may not be fully captured with a single point measurement at the center of a tumor.

Interestingly, abdominal compression may play a role in mediating the interplay effect by improving the regularity of the respiratory waveform and reducing intermittent pauses and irregularities. This factor, however, requires more data and longer respiratory waveforms to assess the stability of the pattern of an extended period of time.

Chapter 7. Interplay Effect: Optimizing plans

7.1 Introduction

Building upon the data and results presented in the previous chapters, the goal here is to determine if modifying the pitch of a plan would reduce the interplay effect. The hypothesis for this study is that a larger pitch will reduce the dose discrepancy between the stationary and motion conditions.

It appears that for most patient respiratory waveforms and tumor amplitudes, the overall clinical impact of the interplay effect is already small on average. There are, however, a few cases where the interplay effect resulted in dosimetric differences of >2%, which is the ASTRO recommended tolerance for an end-to-end dosimetric evaluation for SBRT (36).

7.2 Methods

Using the same phantom and six patient respiratory traces, an SBRT plan was generated using a pitch of 0.487, and prescription dose of 7 Gy to 95% of the ITV. To achieve this, the plan required the use of the 1-cm jaw width instead of the 2.5-cm jaw setting, otherwise the gantry period would be too fast and exceed the limits of the machine. This plan resulted in a significantly longer treatment time (around 10.5 minutes), and had the maximum allowable gantry period of 60 seconds per rotation, which also causes a very slow couch velocity of 0.00782 cm/sec. An A1SL ion chamber was used to measure the dose in the center of the Quasar motion phantom, and GafChromic EBT3 film (Lot#12291501) was used to obtain a 2-dimensional fluence distribution down the center plane of the plastic tumor.

7.3 Results

The dose differences measured with the ion chamber between the stationary and motion conditions were very small. The percent difference for all six cases were less than 1%.

Table 9. Dosimetric differences between stationary and motion conditions for TomoTherapy Plan with 1-cm slice width and pitch of 0.487

Dosimetric Differences for Plan with increased pitch of 0.487					
Case	Tumor Amplitude (cm)	Breath Freq (bpm)	Dose_stationary (Gy)	Dose_motion (Gy)	% difference
1	0.70	22	6.89	6.90	0.1%
2	0.56	15	6.86	6.85	-0.1%
3	2.00	15	6.88	6.87	-0.1%
4	0.57	8	6.88	6.87	-0.1%
5	0.51	19	6.87	6.84	-0.4%
6	2.07	15	7.17	7.13	-0.6%

Table 10. Comparison of Dose Differences between Pitch of 0.1 and 0.487

Dosimetric Differences between Pitch 0.1 and Pitch 0.487				
Case	Dose Difference Pitch 0.1	% Difference	Dose Difference Pitch 0.487	% Difference
1	0.03	0.4%	0.01	0.1%
2	-0.03	-0.4%	-0.01	-0.1%
3	0.03	0.4%	-0.01	-0.1%
4	0.05	0.7%	-0.01	-0.1%
5	-0.03	-0.4%	-0.03	-0.4%
6	-0.32	-4.5%	-0.04	-0.6%

The review of the film data also supports the ion chamber findings, where the penumbra measurements were all very small (less than 1.5 mm) and the variation in flatness was less than 5%, except for Case 6.

Table 11. Film Differences for Pitch 0.487

Planar Film Differences for Plan with increased pitch of 0.487					
Case	Tumor Amplitude (cm)	Breath Freq (bpm)	Penumbra Diff-Lt (cm)	Penumbra Diff-Rt (cm)	Flatness Diff (%)
1	0.70	22	0.11	0.10	1.1
2	0.56	15	0.10	0.08	-3.7
3	2.00	15	0.08	0.03	-3.0
4	0.57	8	0.02	0.02	-4.3
5	0.51	19	0.08	0.09	0
6	2.07	15	1.36	1.16	-16

Profiles for each of the six cases are shown below in Figure 33.

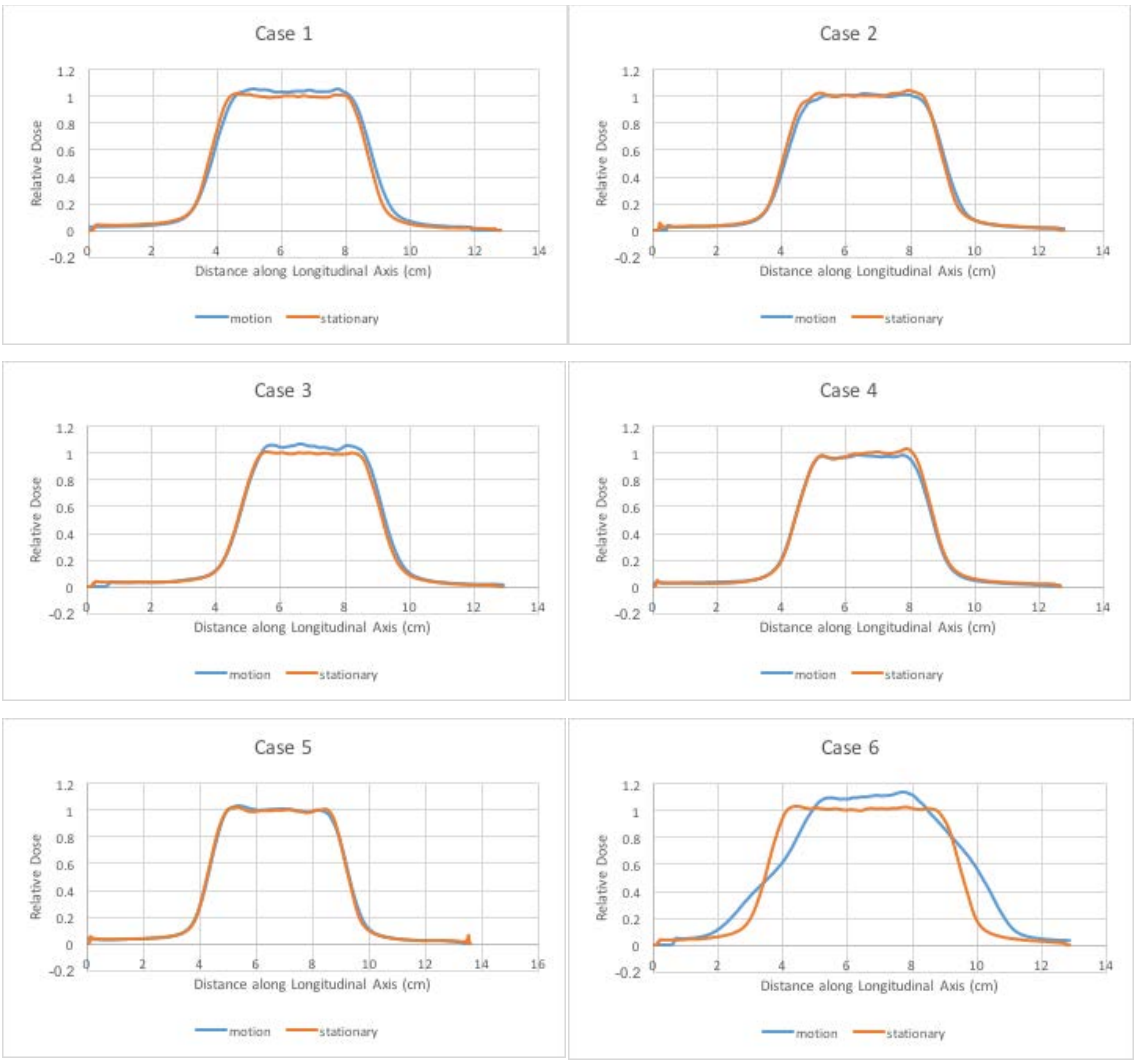

Figure 33 Profiles along the central axis of the film illustrating penumbra and flatness differences between stationary and motion conditions

7.4 Discussion

Despite the very small sample size, the data suggests that increasing the pitch will reduce the impact of the interplay effect. While the ion chamber results were all within 1% of the stationary condition, the limitation of the ion chamber is that it only provides information to a single point, which in this case is the center of the plastic tumor. Film, on the other hand, provides comparative dosimetric information across the central plane bisecting the tumor volume, allowing for visibility into any dose heterogeneities that might otherwise be hidden from the ion chamber. In cases 1-5, despite the small dose differences measured with the ion chamber, there appears to be some 2D variation indicated by the difference in flatness along the central peak in each profile. Case 6 appears to be an exception.

To minimize the interplay effect, the treatment delivery must be slow enough relative to the respiratory frequency such that the tumor will move in and out of the radiation field multiple times per gantry rotation. This slow treatment, however, must be balanced with other clinical considerations such as the discomfort patients experience when lying on a hard, flat table with their arms positioned above their heads for an extended period of time. If the treatment takes too long, patients begin to shift and adjust their bodies to find a more comfortable position, which could lead to significant dosimetric errors, particularly if the tumor abuts a critical organ.

Conversely, the interplay effect appears to be maximized when the gantry period is operating at its fastest. The TomoTherapy system, however, caps the minimum gantry period to 12 seconds per rotation, which would require a consistently slow breath frequency such that the tumor passes through the beam path only once or sometimes not at all. While it is clinically possible that a patient would consistently have an average breath frequency of 5 bpm or less, it is unlikely. However, since it is difficult to accurately predict breathing patterns, it may be prudent to avoid treatment plans with gantry periods of 12 seconds per rotation.

Another option is to maintain an elevated breath frequency. The data presented in this dissertation suggests that abdominal compression increases the average breath frequency by around 1.5 bpm. An additional benefit to abdominal compression is that it appears to improve the regularity of the waveform. Visual comparison of the respiratory waveform points to this trend, albeit for a small sample size of 10 patients.

7.5 Chapter Summary

Slowing the couch velocity and increasing the gantry period, thereby increasing the treatment time, appears to reduce the interplay effect to negligible levels. The disadvantage of this, however, is that this effectively doubles the treatment time. A balance between treatment time and avoiding a low gantry period should be feasible.

Chapter 8 Summary Discussions

8.1 Respiratory Motion Characteristics

Respiratory motion has complex characteristics that are generally cyclical, but may vary considerably over time. The action of breathing introduces a complicated problem for radiation therapy, particularly for SBRT of the lung. While almost all structures in the thorax and abdomen move during respiration, the degree to which they move is largely dependent on the location and surrounding anatomy. As a result, tumors can move as large as 2 or more centimeters, making it challenging to target the tumor while sparing normal, healthy lung. A common method for performing SBRT is to create an ITV, which theoretically encompasses the tumor in all possible locations as measured on 4DCT. If the tumor moves too much, abdominal compression may be applied to try to reduce the extent of motion.

In this dissertation, thirty-five respiratory waveforms from previously treated patients were reviewed and used to simulate a lung tumor moving in a phantom. The proposed technique involved measuring the actual tumor locations on the 4DCTs and using PCA to calculate the maximum tumor displacement. Combining this parameter with the respiratory waveform, a limited model of a patient's moving lung tumor can be created. This was done for each of the 35 respiratory waveforms and formed the basis for exploring the interplay effect for both TomoTherapy imaging and treatment systems.

For the majority of the cases reviewed, this technique worked well. There was overall good validation when comparing the 4DCT studies of the patients and the phantom.

8.2 Interplay Effect

For TomoTherapy treatments, the interplay effect involves the coincidence of breathing induced motion and the synchrony of the treatment couch, gantry, and MLC. As lung tumors move under respiration, they primarily move in the superior-inferior direction, which may result in the tumor moving into and out of the radiation field. Several studies have attempted to characterize this interplay effect using computer simulations and simple geometries, and a few with phantom measurements. All of these studies, however, were primarily focused on conventional radiation therapy fractionation, not SBRT. In the case of SBRT treatments, the interplay effect could affect both the imaging accuracy for tumor localization and reduce the dose delivered to the tumor. These effects could be significant considering the relatively few number of fractions used for SBRT.

8.2.1 TomoTherapy MVCT

The results of the MVCT investigation of the interplay effect demonstrated no notable interplay effects. No correlations between breath frequency and positional shifts nor volume measurements were observed across the cohort. Tumor amplitude does lead to larger motion artifacts, but for setup verification, these positional differences attributed to tumor amplitude were within the 2-mm tolerance margin. The most clinically significant results were that a few scans done in coarse or normal mode that

had positional errors larger than the 2-mm tolerance, although these would likely be accounted for with an additional setup margin of 0.3-1 cm.

Interestingly, abdominal compression may encourage more regular and also shallower breathing that could help improve the imaging accuracy, even for smaller tumor amplitudes. The preliminary data presented here suggests that abdominal compression may improve regularity of the respiratory waveform, although more data would be required to investigate this further.

8.2.2 TomoTherapy SBRT Treatments

The results of the SBRT treatment component of this dissertation are mixed. Lower breath frequencies increased the standard deviation of dose to the tumor. This was both observed within the native-bpm cohort, and validated with data from the 5-bpm measurements. Tumor amplitude was also a strong factor in increasing the variance and showed a moderate correlation with larger penumbra on the film analysis.

The design of this study was particularly novel in the use of the TomoElectrometer Measurement System (TEMS) to visualize the accumulation of dose to the tumor over time, as it moves in and out of the radiation field. The timing of the radiation delivery with the respiratory waveform was visibly evident when comparing different measurements for the same waveform. In addition, the SBRT plan calculated was designed to try to amplify any interplay effects by utilizing the fasted gantry rotation period possible. Even under this scenario, for the majority of respiratory waveforms operating at their native breath frequencies, the ITV approach with a moving internal target appears acceptable. Doses were found to be within 2% and 2mm for the majority of cases.

The caveat to this conclusion, however, is that there were a few cases where the interplay lead to dose discrepancies that exceeded 2%. These differences were exacerbated when the respiratory waveforms were stretched to mimic a 5-bpm breath frequency. This was an important feature of this study as it highlighted the impact that breath frequency may have on the overall treatment accuracy. While patients do not typically breath as slow as 5 bpm, there have been instances where patients will fall asleep during treatment. Given that there is currently no respiratory monitoring system in the TomoTherapy treatment room, it is unknown how different patients breathe from the time of simulation to the time of treatment. Abdominal compression may also play a role in the interplay effect for treatment. A shallower and more regular respiratory waveform would likely reduce any dose discrepancies.

Overall, this study further validates with the ion chamber and film measurements that the interplay effect is likely to have a minimal clinical impact. To ensure optimal dose imaging and dose delivery, SBRT patients should be scanned in fine mode, and SBRT plans should avoid a gantry period of 12 seconds per rotation. In general, a higher breath frequency and lower tumor amplitude are preferable, and so abdominal compression may be an easy way to influence patients' respiratory waveforms.

8.3 Limitations

There are several limitations to this study. One limitation is that the motion phantom is programmable to move only in the cranio-caudal direction. This, however, is not considered a significant limitation because the dominant direction of lung tumor motion is also in the cranio-caudal direction(56). In addition, due to the longitudinal delivery of radiation by the TomoTherapy system, the interplay effect is primarily applicable in the cranio-caudal direction.

A second limitation is the assumption that patients breathe the exact same way during simulation as during treatment. The TomoTherapy system, however, currently does not have an option for integrating a respiratory monitoring system and our department does not have an independent method for monitoring motion at this time. In addition, patient respiratory traces are recorded for varying lengths of time, but are much shorter in duration than the time it takes to deliver a 7 Gy treatment. To maintain phantom motion throughout treatment delivery, the respiratory trace needed to be looped to repeat. This represents a deviation from the clinical scenario since patients do not replicate exactly the same breath patterns in repeating loops.

A third limitation is that the interplay effect may be affected by the synchronization of the start of treatment delivery with particular points in the respiratory cycle, such as full inspiration for example. In clinical practice, however, there is a non-fixed delay between when the TomoTherapy start button is pressed and the actual beam turning on. This delay is due to the system ramping up to the correct gantry speed and ensuring correct gantry position prior to beam delivery, and thus it is currently not possible to synchronize the phases of phantom motion with the beam turning on.

A fourth limitation is that the plastic tumor inside the motion phantom is a simplified model of a lung tumor. Lung tumors are often not spherical and frequently have long thin extensions along the bronchioles. During respiration, it is not uncommon for these tumors to stretch and contract. In addition, many tumors have a smaller diameter than 3 cm. However, the goal of this study is to isolate the relationship between motion and the Tomotherapy system, and the programmable phantom is an appropriate tool for the objectives of this study.

8.4 Closing Remarks

The results of this dissertation demonstrated that while the interplay effect is measurable, the clinical impact is relatively small. This does not mean that it can be ignored, however. Instead, for those cases with larger tumor displacements and slow breath frequencies, a key parameter to note is the gantry period of the treatment plan. Based on this study, avoiding plans that use a 12 second rotation period will help minimize the dosimetric discrepancy due to the interplay effect. Further work can be done with characterizing respiratory patterns and investigating the impact of abdominal compression. A long-term clinical outcomes study could also be performed to determine if there are correlations between treatment failures and cases of larger interplay effect and other associated parameters such as gantry rotation

period, although determining a significant effect may be difficult given that the median age of the treatment population is 77 years.

BIBLIOGRAPHY

1. Non-small Cell Lung Cancer Key Statistics [Internet]. Key statistics for lung cancer. 2016. Available from: http://www.cancer.org/cancer/lungcancer-non-smallcell/detailedguide/non-small-cell-lung-cancer-key-statistics

2. Ettinger DS, Wood DE, Akerley W, Bazhenova LA, Borghaei H, Camidge DR, et al. Non-Small Cell Lung Cancer, Version 4.2016. J Natl Compr Canc Netw [Internet]. 2016 [cited 2016 Nov 19];14(3):255–64. Available from: http://www.jnccn.org/content/14/3/255.short

3. Fakiris AJ, McGarry RC, Yiannoutsos CT, Papiez L, Williams M, Henderson MA, et al. Stereotactic body radiation therapy for early-stage non-small-cell lung carcinoma: four-year results of a prospective phase II study. Int J Radiat Oncol Biol Phys [Internet]. 2009 Nov 1;75(3):677–82. Available from: http://www.ncbi.nlm.nih.gov/pubmed/19251380

4. Chang BK, Timmerman RD. Stereotactic Body Radiation Therapy: A Comprehensive Review. Am J Clin Oncol [Internet]. 2007 Dec [cited 2016 Nov 19];30(6):637–44. Available from: http://content.wkhealth.com/linkback/openurl?sid=WKPTLP:landingpage&an=00000421-200712000-00012

5. Kissick MW, Mackie TR. Task Group 76 Report on “The management of respiratory motion in radiation oncology” [Med. Phys. 33, 3874–3900 (2006)]. Med Phys. 2009;36(12):5721.

6. Zhang F, Kelsey CR, Yoo D, Yin FF, Cai J. Uncertainties of 4-dimensional computed tomography-based tumor motion measurement for lung stereotactic body radiation therapy. Pr Radiat Oncol [Internet]. 2014 Jan;4(1):e59-65. Available from: http://www.ncbi.nlm.nih.gov/pubmed/24621433

7. Koshy M, Malik R, Weichselbaum RR, Sher DJ. Increasing radiation therapy dose is associated with improved survival in patients undergoing stereotactic body radiation therapy for stage i non-small-cell lung cancer. Int J Radiat Oncol Biol Phys [Internet]. 2015 Feb 1;91(2):344–50. Available from: http://www.ncbi.nlm.nih.gov/pubmed/25636759

8. Tudor GS, Harden SV, Thomas SJ. Three-dimensional analysis of the respiratory interplay effect in helical tomotherapy: Baseline variations cause the greater part of dose inhomogeneities seen. Med Phys [Internet]. 2014 Mar;41(3):31704. Available from: http://www.ncbi.nlm.nih.gov/pubmed/24593708

9. Holmes TW, Hudes R, Dziuba S, Kazi A, Hall M, Dawson D. Stereotactic Image-Guided Intensity Modulated Radiotherapy Using the HI-ART II Helical Tomotherapy System. Med Dosim. 2008;33(2):135–48.

10. Shin E, Han Y, Park HC, Sung Kim J, Hwan Ahn S, Suk Shin J, et al. Cumulative dose on fractional delivery of tomotherapy to periodically moving organ: a phantom QA suggestion. Med Dosim [Internet]. 2013 Winter;38(4):359–65. Available from: http://www.ncbi.nlm.nih.gov/pubmed/23769495

11. Woodford C, Yartsev S, Van Dyk J. Image registration of a moving target phantom with helical tomotherapy: effect of the CT acquisition technique and action level proposal. Phys Med Biol [Internet]. 2008 Sep 21;53(18):5093–106. Available from: http://www.ncbi.nlm.nih.gov/pubmed/18723925

12. Kissick MW, Mo X, McCall KC, Schubert LK, Westerly DC, Mackie TR. A phantom model demonstration of tomotherapy dose painting delivery, including managed respiratory motion without motion management. Phys Med Biol [Internet]. 2010 May 21;55(10):2983–95. Available from: http://www.ncbi.nlm.nih.gov/pubmed/20436233

13. Kissick MW, Boswell SA, Jeraj R, Mackie TR. Confirmation, refinement, and extension of a study in intrafraction motion interplay with sliding jaw motion. Med Phys. 2005;32(7):2346.

14. Klein M, Gaede S, Yartsev S. A study of longitudinal tumor motion in helical tomotherapy using a cylindrical phantom. J Appl Clin Med Phys [Internet]. 2013 [cited 2016 Nov 20];14(2). Available from: http://jacmp.org/index.php/jacmp/article/view/4022

15. Society AC. Cancer Facts and Figures 2014. Atlanta: American Cancer Society; 2014.

16. GLOBOCAN 2012: Estimated Cancer Incidence, Mortality and Prevalence Worldwide in 2012 [Internet]. World Health Organization; Available from: http://globocan.iarc.fr

17. Sibley, GS. Radiotherapy for patients with medically inoperable Stage I nonsmall cell lung carcinoma: smaller volumes and higher doses -- a review. Cancer. 1998 Feb 1;82(3):433–8.

18. Timmerman R. Stereotactic Body Radiation Therapy for Inoperable Early Stage Lung Cancer. JAMA [Internet]. 2010 Mar 17 [cited 2017 Mar 16];303(11):1070. Available from: http://jama.jamanetwork.com/article.aspx?doi=10.1001/jama.2010.261

19. Jeremic B, Shibamoto Y, Acimovic L, Nikolic N, Dagovic A, Aleksandrovic J, et al. Second cancers occurring in patients with early stage non-small-cell lung cancer treated with chest radiation therapy alone. J Clin Oncol. 2001 Feb 15;19(4):1056–63.

20. Pennathur A, Luketich JD, Heron DE, Schuchert MJ, Bianco V, Clump D, et al. Stereotactic Radiosurgery/Stereotactic Body Radiotherapy for Recurrent Lung Neoplasm: An Analysis of Outcomes in 100 Patients. Ann Thorac Surg [Internet]. 2015 Dec [cited 2017 Mar 20];100(6):2019–24. Available from: http://linkinghub.elsevier.com/retrieve/pii/S0003497515007882

21. Owen D, Olivier KR, Mayo CS, Miller RC, Nelson K, Bauer H, et al. Outcomes of Stereotactic Body Radiotherapy (SBRT) treatment of multiple synchronous and recurrent lung nodules. Radiat Oncol [Internet]. 2015 [cited 2017 Mar 20];10(1):43. Available from: http://www.ro-journal.com/content/10/1/43

22. Park S, Urm S, Cho H. Analysis of Biologically Equivalent Dose of Stereotactic Body Radiotherapy for Primary and Metastatic Lung Tumors. Cancer Res Treat [Internet]. 2014 Jul 17 [cited 2017 Mar 24];46(4):403–10. Available from: http://e-crt.org/journal/view.php?doi=10.4143/crt.2013.168

23. Inoue T, Shimizu S, Onimaru R, Takeda A, Onishi H, Nagata Y, et al. Clinical Outcomes of Stereotactic Body Radiotherapy for Small Lung Lesions Clinically Diagnosed as Primary Lung Cancer on Radiologic Examination. Int J Radiat Oncol [Internet]. 2009 Nov [cited 2017 Mar 25];75(3):683–7. Available from: http://linkinghub.elsevier.com/retrieve/pii/S036030160803808X

24. Bezjak, A., Seamless Phase I/II Study of Stereotactic Lung Radiotherapy (SBRT) for Early Stage, Centrally Located, Non-Small Cell Lung Cancer (NSCLC) in Medically Inoperable Patients. RTOG0813. Current version date: 2015 Jun 8. https://www.rtog.org/ClinicalTrials/ProtocolTable/StudyDetails.aspx?study=0813

25. Kim M-S, Kim W, Park IH, Kim HJ, Lee E, Jung J-H, et al. Radiobiological mechanisms of stereotactic body radiation therapy and stereotactic radiation surgery. Radiat Oncol J [Internet]. 2015 [cited 2017 Mar 16];33(4):265. Available from: http://e-roj.org/journal/view.php?doi=10.3857/roj.2015.33.4.265

26. Brown JM, Carlson DJ, Brenner DJ. The Tumor Radiobiology of SRS and SBRT: Are More Than the 5 Rs Involved? Int J Radiat Oncol [Internet]. 2014 Feb [cited 2017 Mar 16];88(2):254–62. Available from: http://linkinghub.elsevier.com/retrieve/pii/S0360301613028605

27. Song CW, Kim M-S, Cho LC, Dusenbery K, Sperduto PW. Radiobiological basis of SBRT and SRS. Int J Clin Oncol [Internet]. 2014 Aug [cited 2017 Mar 16];19(4):570–8. Available from: http://link.springer.com/10.1007/s10147-014-0717-z

28. Maquilan G, Timmerman R. Stereotactic Body Radiation Therapy for Early-Stage Lung Cancer. Cancer J [Internet]. 2016 [cited 2017 Mar 16];22(4):274–279. Available from: http://journals.lww.com/journalppo/Abstract/2016/07000/Stereotactic_Body_Radiation_Therapy_for.7.aspx

29. Benedict SH, Yenice KM, Followill D, Galvin JM, Hinson W, Kavanagh B, et al. Stereotactic body radiation therapy: The report of AAPM Task Group 101. Med Phys. 2010;37(8):4078.

30. Marcenaro M, Vagge S, Belgioia L, Agnese D, Lamanna G, Mantero E, et al. Ablative or palliative stereotactic body radiotherapy with helical tomotherapy for primary or metastatic lung tumor. Anticancer Res [Internet]. 2013 [cited 2017 Mar 24];33(2):655–660. Available from: http://ar.iiarjournals.org/content/33/2/655.short

31. Vedam SS, Keall PJ, Kini VR, Mostafavi H, Shukla HP, Mohan R. Acquiring a four-dimensional computed tomography dataset using an external respiratory signal. Phys Med Biol [Internet]. 2002 [cited 2016 Dec 1];48(1):45. Available from: http://iopscience.iop.org/article/10.1088/0031-9155/48/1/304/meta

32. Ionascu D, Jiang SB, Nishioka S, Shirato H, Berbeco RI. Internal-external correlation investigations of respiratory induced motion of lung tumors: Correlation of respiratory induced motion of lung tumors. Med Phys [Internet]. 2007 Sep 19 [cited 2017 Mar 20];34(10):3893–903. Available from: http://doi.wiley.com/10.1118/1.2779941

33. Hoisak JDP, Sixel KE, Tirona R, Cheung PCF, Pignol J-P. Correlation of lung tumor motion with external surrogate indicators of respiration. Int J Radiat Oncol [Internet]. 2004 Nov [cited 2016 Nov 21];60(4):1298–306. Available from: http://linkinghub.elsevier.com/retrieve/pii/S0360301604020681

34. Respiratory Motion Management for CT [Internet]. The Netherlands: Philips Healthcare; 2013 p. 1–6. Available from: http://www.philips.com/BigBoreCT

35. Lu W, Parikh PJ, Hubenschmidt JP, Bradley JD, Low DA. A comparison between amplitude sorting and phase-angle sorting using external respiratory measurement for 4D CT. Med Phys [Internet]. 2006 [cited 2016 Nov 21];33(8):2964. Available from: http://scitation.aip.org/content/aapm/journal/medphys/33/8/10.1118/1.2219772

36. Solberg TD, Balter JM, Benedict SH, Fraass BA, Kavanagh B, Miyamoto C, et al. Quality and Safety Considerations in Stereotactic Radiosurgery and Stereotactic Body Radiation Therapy. Pr Radiat Oncol [Internet]. 2011 Aug [cited 2017 Mar 24];(Supplemental Material). Available from: https://pdfs.semanticscholar.org/f057/538e0c2700aa4bb15825cbf0d6d46ffb31b5.pdf

37. Moldovan M, Fontenot JD, Gibbons JP, Lee TK, Rosen II, Fields RS, et al. Investigation of Pitch and Jaw Width to Decrease Delivery Time of Helical Tomotherapy Treatments for Head and Neck Cancer. Med Dosim [Internet]. 2011 Dec [cited 2017 Mar 17];36(4):397–403. Available from: http://linkinghub.elsevier.com/retrieve/pii/S0958394710001901

38. Chen M, Chen Y, Chen Q, Lu W. Theoretical analysis of the thread effect in helical TomoTherapy. Med Phys [Internet]. 2011 Nov;38(11):5945–60. Available from: http://www.ncbi.nlm.nih.gov/pubmed/22047359

39. Westerly DC, Soisson E, Chen Q, Woch K, Schubert L, Olivera G, et al. Treatment planning to improve delivery accuracy and patient throughput in helical tomotherapy. Int J Radiat Oncol Biol

Phys [Internet]. 2009 Jul 15;74(4):1290–7. Available from: http://www.ncbi.nlm.nih.gov/pubmed/19394157

40. De Kerf G, Van Gestel D, Mommaerts L, Van den Weyngaert D, Verellen D. Evaluation of the optimal combinations of modulation factor and pitch for Helical TomoTherapy plans made with TomoEdge using Pareto optimal fronts. Radiat Oncol [Internet]. 2015 Dec [cited 2017 Mar 17];10(1). Available from: http://www.ro-journal.com/content/10/1/191

41. Binny D, Lancaster CM, Harris S, Sylvander SR. Effects of changing modulation and pitch parameters on tomotherapy delivery quality assurance plans. J Appl Clin Med Phys. 2015;16(5).

42. Kissick MW, Fenwick J, James JA, Jeraj R, Kapatoes JM, Keller H, et al. The helical tomotherapy thread effect: The helical tomotherapy thread effect. Med Phys [Internet]. 2005 Apr 27 [cited 2017 Mar 17];32(5):1414–23. Available from: http://doi.wiley.com/10.1118/1.1896453

43. Hodge W, Tomé WA, Jaradat HA, Orton NP, Khuntia D, Traynor A, et al. Feasibility report of image guided stereotactic body radiotherapy (IG-SBRT) with tomotherapy for early stage medically inoperable lung cancer using extreme hypofractionation. Acta Oncol [Internet]. 2006 Jan [cited 2017 Mar 17];45(7):890–6. Available from: http://www.tandfonline.com/doi/full/10.1080/02841860600907329

44. Weyh A, Konski A, Nalichowski A, Maier J, Lack D. Lung SBRT: dosimetric and delivery comparison of RapidArc, TomoTherapy, and IMRT. J Appl Clin Med Phys. 2013;14(4).

45. Chi A, Jang SY, Welsh JS, Nguyen NP, Ong E, Gobar L, et al. Feasibility of Helical Tomotherapy in Stereotactic Body Radiation Therapy for Centrally Located Early Stage Non–Small-Cell Lung Cancer or Lung Metastases. Int J Radiat Oncol [Internet]. 2011 Nov [cited 2016 Nov 19];81(3):856–62. Available from: http://linkinghub.elsevier.com/retrieve/pii/S0360301610036746

46. Chi A, Ma P, Fu G, Hobbs G, Welsh JS, Nguyen NP, et al. Critical structure sparing in stereotactic ablative radiotherapy for central lung lesions: helical tomotherapy vs. volumetric modulated arc therapy. PLoS One [Internet]. 2013;8(4):e59729. Available from: http://www.ncbi.nlm.nih.gov/pubmed/23577071

47. Chaudhari SR, Goddu SM, Rangaraj D, Pechenaya OL, Lu W, Kintzel E, et al. Dosimetric variances anticipated from breathing- induced tumor motion during tomotherapy treatment delivery. Phys Med Biol [Internet]. 2009 Apr 21;54(8):2541–55. Available from: http://www.ncbi.nlm.nih.gov/pubmed/19349658

48. Yu CX, Jaffray DA, Wong, J. W. The effects of intra-fraction organ motion on the delivery of dynamic intensity modulation. Phys Med Biol. 1998;43(1):91–104.

49. Yang JN, Mackie TR, Reckwerdt P, Deasy JO, Thomadsen BR. An investigation of tomotherapy beam delivery. Med Phys [Internet]. 1997 [cited 2017 Mar 26];24(3):425–436. Available from: http://onlinelibrary.wiley.com/doi/10.1118/1.597909/full

50. Tsunashima Y, Sakae T, Shioyama Y, Kagei K, Terunuma T, Nohtomi A, et al. Correlation between the respiratory waveform measured using a respiratory sensor and 3D tumor motion in gated radiotherapy. Int J Radiat Oncol [Internet]. 2004 Nov [cited 2017 Mar 20];60(3):951–8. Available from: http://linkinghub.elsevier.com/retrieve/pii/S0360301604010831

51. Yan H, Yin F-F, Zhu G-P, Ajlouni M, Kim JH. The correlation evaluation of a tumor tracking system using multiple external markers: The correlation analysis of a tumor tracking system. Med Phys [Internet]. 2006 Oct 16 [cited 2017 Mar 20];33(11):4073–84. Available from: http://doi.wiley.com/10.1118/1.2358830

52. Kanagaki B, Read PW, Molloy JA, Larner JM, Sheng K. A motion phantom study on helical tomotherapy: the dosimetric impacts of delivery technique and motion. Phys Med Biol [Internet]. 2007 Jan 7 [cited 2017 Mar 5];52(1):243–55. Available from: http://stacks.iop.org/0031-9155/52/i=1/a=016?key=crossref.a7785c6963699a329248df7561f6243c

53. Kim B, Chen J, Kron T, Battista J. Motion-induced dose artifacts in helical tomotherapy. Phys Med Biol. 2009 Sep 4;54(2009):5707–34.

54. Beddar AS, Kainz K, Briere TM, Tsunashima Y, Pan T, Prado K, et al. Correlation between internal fiducial tumor motion and external marker motion for liver tumors imaged with 4D-CT. Int J Radiat Oncol [Internet]. 2007 Feb [cited 2016 Nov 21];67(2):630–8. Available from: http://linkinghub.elsevier.com/retrieve/pii/S0360301606032391

55. Giglioli FR, Strigari L, Ragona R, Borzì GR, Cagni E, Carbonini C, et al. Lung stereotactic ablative body radiotherapy: A large scale multi-institutional planning comparison for interpreting results of multi-institutional studies. Phys Med [Internet]. 2016 Apr [cited 2017 Mar 20];32(4):600–6. Available from: http://linkinghub.elsevier.com/retrieve/pii/S1120179716300102

56. Knybel L, Cvek J, Molenda L, Stieberova N, Feltl D. Analysis of Lung Tumor Motion in a Large Sample: Patterns and Factors Influencing Precise Delineation of Internal Target Volume. Int J Radiat Oncol [Internet]. 2016 Nov [cited 2016 Nov 18];96(4):751–8. Available from: http://linkinghub.elsevier.com/retrieve/pii/S036030161633067X